Dynamics of the Most Probable Composition Fluctuations of "Real" Diblock Copolymers near the Ordering Transition

K. Chrissopoulou,[†] V. A. Pryamitsyn,[‡,#] S. H. Anastasiadis,[*,†,§] G. Fytas,[*,†] A. N. Semenov,[‡] M. Xenidou,[⊥,%] and N. Hadjichristidis[⊥,†]

Foundation for Research and Technology−Hellas, Institute of Electronic Structure and Laser, P.O. Box 1527, 711 10 Heraklion Crete, Greece; Department of Applied Mathematics, University of Leeds, Leeds LS2 9JT, U.K.; Physics Department, University of Crete, 710 03 Heraklion Crete, Greece; and Department of Chemistry, University of Athens, 157 01 Zografou Athens, Greece

Received September 6, 2000; Revised Manuscript Received November 27, 2000

ABSTRACT: Semidilute solutions of ultrahigh molecular weight diblocks in a nonselective good solvent allow investigation of the dynamic structure factor $S(q,t)$ by photon correlation spectroscopy for wavevectors q in the vicinity (and on both sides) of the maximum of the static structure factor q^* ($0.2 \leq q/q^* \leq 2.1$) as a function of copolymer concentration in the ordering regime. The relaxation rate of the short-range composition fluctuations at q^*, $\Gamma(q^*)$, shows a significant slowing down relative to the respective long-range ones at low wavevectors; as the ordering transition is approached, this slowing down becomes very pronounced. $\Gamma(q^*)$ has been anticipated to influence the low-frequency rheological behavior of disordered diblocks. Additionally, a general theory for the $S(q,t)$ of entangled polydisperse diblock copolymers is developed in the framework of the random phase approximation assuming reptation dynamics. Although both internal diffusion and ordinary interdiffusion contribute to the dynamics of long-range composition fluctuations, it is the internal diffusion at finite wavevectors near q^*, which is affected by approaching the ordering transition from the disordered state. Nevertheless, composition polydispersity causes a coupling of these relaxation modes, which hinders their identification over the whole q range. The theoretical results are favorably compared with the experimental data.

I. Introduction

In any homogeneous multiconstituent polymer system, either an A/B blend or an A−B block copolymer, composition fluctuations are thermally induced; i.e., the volume fraction of, e.g., A at a position **r** at time t is different from the average composition

$$\delta\phi_A(\mathbf{r},t) = \phi_A(\mathbf{r},t) - \bar{\phi}_A = -\delta\phi_B(\mathbf{r},t) \qquad (1)$$

These composition fluctuations define the dynamic structure factor

$$S(\mathbf{q},t) = \langle \delta\phi_A(\mathbf{q},0)\, \delta\phi_A(-\mathbf{q},t)\rangle \qquad (2)$$

where $\delta\phi_A(\mathbf{q},t)$ is the Fourier transform of $\delta\phi_A(\mathbf{r},t)$, **q** is the wavevector, and $\langle\cdots\rangle$ denotes the ensemble average. The relaxation of $S(\mathbf{q},t)$, i.e., the dynamics of composition fluctuations, is determined by the collective relative motion of the species, whereas the relaxation of the most probable composition fluctuations is significantly influenced by the thermodynamic interactions between the dissimilar components.

For binary polymer blends (intermolecular mixtures), the most probable composition fluctuations are long-ranged (i.e., the maximum of the static structure factor $S(q)$ is at $q \to 0$), and the relaxation of $S(q,t)$ proceeds via the well-known interdiffusion process. As the macrophase separation is approached, the unfavorable thermodynamic interactions lead to a significant thermodynamic slowing down of the interdiffusion over long distances.[1]

For diblock copolymers (intramolecular mixtures), which consist of two covalently bonded linear sequences of chemically dissimilar species A and B, $S(q)$ exhibits a maximum at a finite wavevector,[2] $q^* \sim O(1/R_g)$, where R_g is the radius of gyration; this maximum increases in magnitude and becomes narrower as the unfavorable enthalpic interactions lead toward the disorder-to-order transition (ODT).[2,3] The relaxation of $S(\mathbf{q},t)$ proceeds via the collective relative motion of the two blocks giving rise to the "internal" copolymer mode,[4,5] investigated before[6−13] in the melt[8] and in semidilute solutions[6,7,9−13] in a common good solvent.[14] For $qR_g \ll 1$, the decay rate of the internal process is purely kinetic and is determined by the longest chain conformational relaxation time; i.e., the effects of the thermodynamic interactions are negligible.[7−10] For $q \to q^*$, the effects of the proximity to ODT begin to be evident[11,12] as the increase of $S(q)$ is accompanied by a retardation of the dynamics; the $0.23 < q/q^* < 1.$ range was studied therein. The $1.4 \leq q/q^* \leq 9.1$ regime was recently investigated by neutron spin echo for $10^{-10} < t < 2 \times 10^{-8}$ s, where no significant thermodynamic effects were observed.[15] Besides the relative motion of the two blocks (internal diffusion), the relative motion of different chains (interdiffusion) may significantly contribute or even dominate at large scales ($qR_g \ll 1$) if the copolymer is compositionally polydisperse; in practice, all real polymer systems are polydisperse. This motion leads to an additional "polydispersity" (or "heterogeneity") diffusive process, which has been observed before[8−10,13] and identified[9,16,17] with the copolymer self-diffusivity; it is observed due to the finite inherent composition poly-

[†] Foundation for Research and Technology−Hellas.
[‡] University of Leeds.
[§] University of Crete.
[⊥] University of Athens.
* To whom correspondence should be addressed.
[#] Present address: University of Oregon, Department of Chemistry and Institute of Theoretical Science, Eugene, OR 97403.
[%] Present address: ExxonMobil Research & Engineering Co., Corporate Strategic Research Labs., Annandale, NJ 08801.

10.1021/ma001541b CCC: $20.00
Published on Web 02/22/2001

dispersity of the copolymer. An extensive account on the quite-intense recent research work on copolymer dynamics is provided in recent reviews.[18]

On the theoretical side, so far $S(q,t)$ in diblock copolymers has been studied for monodisperse systems[4,5,12,15] (for Rouse[5,15] or for entangled[4,12] chains) as well as for polydisperse diblocks for $qR_g \ll 1$.[9,16] Experimental data and theory quantitatively agree on the existence and characteristics of two modes for $qR_g \ll 1$: an internal mode with intensity $I_{int} \propto N^2q^2$ and rate $\Gamma_{int}(q) \propto \tau_1^{-1}\, q^0$; a polydispersity-induced self-diffusion mode with intensity $I_p \propto \kappa_0 N q^0$ and rate $\Gamma_p(q) \approx D_s q^2$ (N is the total number of copolymer segments, τ_1 the longest relaxation time, D_s the self-diffusivity, and κ_0 the variance of the composition polydispersity). For a monodisperse diblock, the self-diffusion mode has identically zero amplitude. Moreover, another weak process observed[11,12] for entangled chains was assigned to Rouse-like chain fluctuations inside their reptation tubes; the large N made the Rouse mode observable whereas the thermodynamic effects on this process were less important.[12]

The approach to the ODT dramatically affects the rheological properties of block copolymers.[3] The rheological signature of strong composition fluctuations is the failure of the time−temperature superposition to generate master curves of the dynamic moduli with frequency ω; more specifically, the dynamic storage modulus, $G'(\omega)$, develops a shoulder at the beginning of the terminal region with the conventional terminal regime ($G'(\omega) \propto \omega^2$), appearing only below a characteristic frequency $\hat{\omega} \ll 1/\tau_1$. A mean-field theory evaluation of $\hat{\omega}$ showed[19] that it is determined by the relaxation rate of composition fluctuations, $\Gamma(q)$, and is dominated by that at q^*, $\Gamma(q^*)$; this rate is being probed in the present investigation.

For the investigation of the $qR_g \approx O(1)$ regime with the broad time range (10^{-7}−10^3 s) of dynamic light scattering ($3.7 \times 10^{-3}\text{nm}^{-1} < q < 3.4 \times 10^{-2}\text{nm}^{-1}$), very high molecular weight copolymers are needed.[11−13] The phase state of diblocks of composition f_A (volume fraction of component A) is controlled[2,3] by χN, where χ the interaction parameter: for $\chi N \sim O(10)$, the disorder-to-order transition (ODT) leads from a disordered state at low values of χN toward a microphase-segregated state at higher χN with long-range compositional order. In solution in a common good solvent,[20−24] the unfavorable interactions are diluted and the ODT can be accessed even for high N's by modifying concentration ϕ. In semidilute solutions, χN is renormalized[9,21,24] as $\chi^* \cong \chi\phi^{(1-z)/(3\nu-1)} = \chi\phi^{1.59}$, with $z = -0.225$, ν the Flory exponent ($\nu = 0.59$ in good solvents), and ϕ the polymer volume fraction in solution.

In this paper, the dynamics of composition fluctuations of disordered diblock copolymers is investigated both experimentally and theoretically for wavevectors q in the vicinity and on both sides of the wavevector at the maximum of the static structure factor, q^*. Ultrahigh molecular weight almost symmetric polystyrene-*block*-polyisoprene diblocks have been synthesized and utilized in semidilute solution in the almost neutral good solvent toluene in order to access the investigation of the dynamic structure factor $S(q,t)$ by photon correlation spectroscopy in the range $0.2 \le q/q^* \le 2.1$ as the ODT is approached. A main mode of relaxation was experimentally resolved for these diblocks with characteristics apparently resembling a mixed "internal" and "polydispersity" mode: intensity $I(q)$ approaching a constant and rate $\Gamma(q)$ proportional to q^2 for $qR_g \ll 1$ but exhibiting the effects of thermodynamics for $q \sim q^*$. As q increases toward q^*, the intensity increases and the effective diffusion coefficient $D(q) = \Gamma(q)/q^2$ decreases. The relaxation of the short-range composition fluctuations at q^* is significantly retarded relative to its respective long-range value at low wavevectors, which mirrors the substantial increase of $I(q)$. As the ODT is approached, this slowing down becomes dramatically pronounced. A theory is developed for the $S(q,t)$ of entangled "real" (polydisperse) diblock copolymers in the framework of the random phase approximation (RPA) and assuming the classical reptation model.[25−27] Both intensities and relaxation rates of the main relaxation modes are predicted for an arbitrary q and for any degree of composition polydispersity. The modes of relaxation are significantly influenced by the composition polydispersity even for very small polydispersities, whereas it is not possible to distinguish between the internal diffusion and the polydispersity-induced interdiffusion modes over the whole q range due to their coupling. Both intramolecular breathing motions and ordinary interdiffusion are found to contribute to the dynamics of long-range (low-q) composition fluctuations with relative weights depending on polydispersity; however, it is the intramolecular motion (internal diffusion) at finite wavevectors near q^* that is mainly affected by approaching the ODT. The theoretical results are favorably compared with the experimental data.

This article is arranged as follows: Following the experimental section II, the experimental results are shown in section III. The complete new theoretical approach is presented in section IV, and the results are discussed in relation to the theory in section V. Finally, the concluding remarks constitute section VI.

II. Experimental Section

Materials. The synthesis of the ultrahigh molecular weight polystyrene-*block*-poly(1,4-isoprene) diblock copolymers was performed at room temperature in evacuated, *n*-BuLi washed, and benzene rinsed glass reactor, provided with constrictions and break-seals, using *sec*-BuLi as initiator, similarly to the procedure outlined previously.[11,12] Extra purification for monomers, initiator, and solvents was required due to the very low initiator concentration needed ($\sim O(10^{-5})$ mol for 10 g of copolymer), which was carried out in an apparatus purged with *n*-BuLi. Dibutylmagnesium was used for the purification of styrene (Merck) and *n*-BuLi for isoprene (Fluka). Finally, the purified monomers were distilled in ampules purged with *n*-BuLi. The *sec*-butyllithium initiator was prepared from *sec*-butyl chloride and lithium dispersion. Following this procedure, the initiator was diluted in an apparatus, purged with *n*-BuLi, with calibrated ampules. Initially, the polystyryllithium block was prepared, and a small aliquot was removed for characterization (Figure 1a,c). The polymerization was completed after the addition of the isoprene monomer and took 2 days.

Fractionation of the final diblock copolymer was performed, in several steps, by adding methanol (nonsolvent) to the copolymer solution (~0.1 vol %) in a mixture 1:1 by volume of toluene (solvent for both blocks) and hexane (solvent for PI) in order to remove the homopolymer polystyrene procured due to the expected termination of the polystyryllithium by the minimal (yet unavoidable) impurities in the added isoprene. The fractionation was monitored by size exclusion chromatography (SEC, THF, 30 °C) with differential refractive index and UV detector operating at 266 nm. (The UV detector at 266 nm monitors only the polystyrene part of the copolymer.)

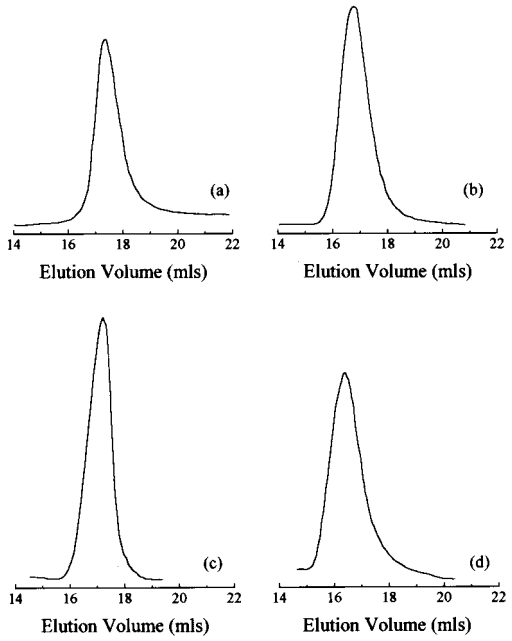

Figure 1. Size exclusion chromatography of (a) the styrene precursor of SI-2M50, (b) the SI-2M50 diblock copolymer, (c) the styrene precursor of SI-3M50, and (d) the SI-3M50 diblock copolymer.

Table 1. Sample Characteristics

sample	M_w[a] ($\times 10^6$)	M_w/M_n	w_{PS}[b]	N[c]	f_{PS}[d]	c^*[e] ($\times 10^{-3}$) (g/mL)	ϕ_{ODT}[f]
SI-2M50	2.03	1.12	0.417	24 479	0.383	2.0	~0.046
SI-3M50	3.00	1.18	0.435	36 086	0.400	1.2	~0.026

[a] By low-angle laser light scattering in THF. [b] Polystyrene weight fraction. [c] Based on average segmental volume. [d] Polystyrene volume fraction. [e] Estimated from dynamic light scattering in the dilute and the crossover regimes. [f] Obtained from polarized and depolarized dynamic light scattering.

The impurities are very influential due to the active centers. The terminated polystyrene precursor was removed by the fractionation, as shown in the SEC traces of Figure 1b,d.

Low-angle laser light scattering (THF, 25 °C), laser differential refractometry (THF, 25 °C, dn/dc = 0.150 mL/g), ^{1}H NMR ($CDCl_3$, 30 °C), and UV (THF, 269 nm) measurements were performed for molecular and compositional characterization. The characteristics of the diblock copolymers are shown in Table 1.

A very low concentration (<0.3 wt %) copolymer solution in HPLC grade toluene solvent is initially prepared and filtered through a 0.22 μm Millipore filter directly into the dust-free light scattering cell (10 mm). During the measurements, the cell was closed airtight to avoid evaporation of toluene. The concentration was checked before and after each measurement by weighing the solution. The concentration is then gradually increased by very slow evaporation of small amounts of solvent (to ensure equilibrium) and weighing the resulting solutions. All the concentrations reported here are well above the overlap concentration c^*, estimated from dynamic light scattering in the dilute and the crossover regimes.

Photon Correlation Spectroscopy (PCS). The autocorrelation function of the polarized light scattering intensity, $G_{VV}(q,t) = \langle I_{VV}(q,t)\, I_{VV}(q,0)\rangle/\langle I_{VV}(q,0)\rangle^2$ (with $\langle I_{VV}(q,0)\rangle$ the mean light scattering intensity), is measured at different scattering angles, θ, using an ALV spectrophotometer and an ALV-5000 full digital correlator over the time range $10^{-7}-10^3$ s. Both the incident beam from an Adlas diode pumped Nd:YAG laser (with wavelength $\lambda = 532$ nm and single mode intensity 100 mW) and the scattering beam were polarized perpendicular (V) to the scattering plane. $q = (4\pi n/\lambda)\sin(\theta/2)$ is the magnitude of the scattering vector, with n the refractive index of the medium. Measurements were performed for scattering angles $12° \le \theta \le 150°$, i.e., for 3.7×10^{-3} nm$^{-1} \le q \le 3.4 \times 10^{-2}$ nm^{-1}. In quasi-elastic light scattering under homodyne conditions, $G_{VV}(q,t)$ is related to the desired field correlation function, $C(q,t)$, by

$$C(q,t) = \{[G_{VV}(q,t) - 1]/f^*\}^{1/2} \tag{3}$$

where f^* is an experimental factor calculated by means of a standard. The amplitude (≤ 1) of the $C(q,t)$ is the fraction of $\langle I_{VV}(q,0)\rangle$ with decay times slower than about 10^{-7} s.

When more than one relaxation process are present in the experimental correlation functions, they are analyzed by performing the inverse Laplace transform (ILT) of $C(q,t)$, without any assumption of the shape of the distribution function $L(\ln \tau)$ but only assuming a superposition of exponentials:

$$C(q,t) = \int_{-\infty}^{\infty} L(\ln \tau)\, \exp[-t/\tau]\, \mathrm{d}(\ln \tau) \tag{4}$$

This determines a continuous spectrum of relaxation times $L(\ln \tau)$; the average times obtained from the peaks of $L(\ln \tau)$ are used to determine the characteristic relaxation times, whereas the integral under the peaks of $L(\ln \tau)$ is the fraction of the total light scattering intensity associated with the specific relaxation. For comparison between different $C(q,t)$, the distributions $L(\ln \tau)$ are shown multiplied by the total light scattering intensity reduced to that of toluene, I_t, i.e., as $I_t L(\ln \tau)$.

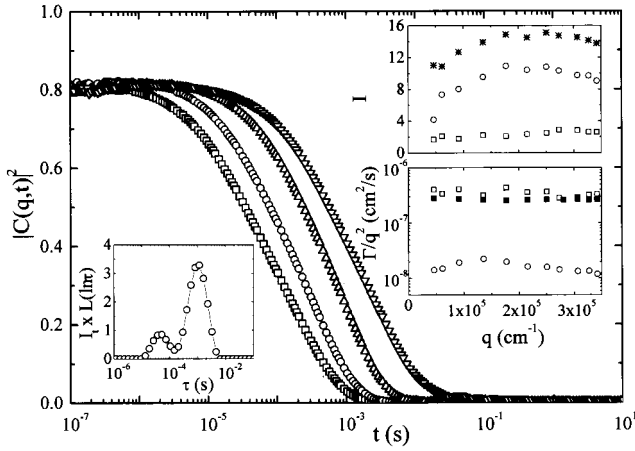

Figure 2. Net intensity autocorrelation functions $|C(q,t)|^2$ of a 1.26 wt % SI-2M50 solution in toluene at 20 °C for scattering angles $\theta = 150°$ (□), 90° (○), 45° (△), and 30° (▽). The left inset shows a typical distribution of relaxation times $L(\ln \tau)$ for $\theta = 90°$ multiplied by the total scattered intensity reduced by that of toluene, I_t. The right inset shows the wavevector dependence of the intensities I and effective diffusion coefficients $D = \Gamma/q^2$ for the cooperative (□) and the internal (○) modes together with the total scattered intensity reduced by the intensity of toluene (*). The solid squares (■) are the cooperative diffusion coefficients for a 1.22 wt % PS-2M/toluene solution.

III. Experimental Results

Figure 2 shows the net polarized intensity autocorrelation functions for the 1.26 wt % SI-2M50 solution in toluene for different scattering angles; the copolymer concentration is low enough so that the copolymer is very far from the ordering transition ($\chi^* N \approx 1.3$). The shape of the correlation functions (being broader than a single-exponential decay) as well as the distributions of relaxation times (shown in the left inset for $\theta = 90°$) indicates the existence of two relaxation processes contributing to the experimental $C(q,t)$. The faster mode, with intensity independent of the wavevector and rate

proportional to q^2 (right insets of Figure 2), corresponds to the relaxation of total concentration fluctuations[14] similarly to semidilute homopolymer solutions; i.e., it is due to the well-known cooperative diffusion. This process has been observed before for semidilute copolymer solutions[7,9−13] and predicted theoretically.[5] Actually, its diffusion coefficient $D = \Gamma/q^2$ superimposes with that for the cooperative diffusion of a polystyrene homopolymer (PS-2M: $M_w = 2.12 \times 10^6$, $M_w/M_n = 1.16$, Polymer Source) solution in toluene, shown in the lower right inset for a 1.22 wt % concentration. Moreover, the intensity of the cooperative diffusion mode for the PS-2M/toluene is about a factor of 3.5 higher than that of SI-2M50/toluene in accordance with their mean refractive indices vs that of toluene. Therefore, the fast process, which is not diblock copolymer specific, is the cooperative diffusion and will not be further discussed in the present paper.

The characteristics of the slower process contributing to the correlation functions of Figure 2 are peculiar: the process exhibits a q^2-dependent relaxation rate (thus, a q-independent effective diffusion coefficient $D = \Gamma/q^2$, lower right inset) together with a nonmonotonic q dependence of its intensity which shows a maximum at a finite wavevector, $q^* \approx 2.5 \times 10^{-2}$ nm^{-1} and a nonzero intercept (upper right inset); the total scattering intensity (also shown in the upper right inset) follows the q dependence of this slower process. The dependence of the intensity on the wavevector for the slower process forces one to relate the mode to the predicted[5,12] internal copolymer mode. However, theory for monodisperse diblocks for $q \ll q^*$ predicts a q-independent relaxation rate for the internal mode, whereas, for low molecular weight diblocks, the diffusive process observed at low qR_g's possesses a q-independent intensity with the mode assigned to the "polydispersity" process. Therefore, even for concentrations far away from the transition, this process apparently exhibits intermediate characteristics between the two processes observed before (even for $qR_g \leq 1$ away from the ODT[13]). The behavior at low concentrations for the SI-3M50 copolymer are exactly analogous with that of Figure 2 with the maximum of the intensity appearing at $q^* \approx 1.7 \times 10^{-2}$ nm^{-1} in accordance with its higher molecular weight.

As the copolymer concentration in the solution increases and the ordering transition is approached, the picture of Figure 2 is modified. Figure 3 shows the net polarized intensity autocorrelation functions for SI-2M50/toluene solutions of different concentrations at $q = 2.5 \times 10^{-2}$ nm$^{-1} \approx q^*$. The distributions $I_tL(\ln \tau)$ are shown in the insets for the lower and the higher concentrations. A significant increase of the intensity of the slower mode is observed (notice the different scales of the insets) as $\phi \rightarrow \phi_{ODT}$, which is accompanied by a significant slowing down of the dynamics at this finite wavevector q^*. In this concentration regime, as ϕ increases by only a factor of about 3, the relaxation time of the main mode becomes slower by almost 3 orders of magnitude whereas its intensity increases by almost the same factor; the respective self-diffusion coefficient decreases by only 1 order of magnitude in this range (see below). It is noted that the highest concentration shown is very close ($\chi^*N \approx 9.22$) to the critical one for microphase separation (for this polydispersity $(\chi^*N)_s \approx 9.26$, see below).

The close proximity to the ODT as the concentration increases is also expressed in the wavevector dependence of the intensity correlation functions. For example, Figure 4 shows the net intensity autocorrelation functions for a 2.6 wt % SI-3M50 solution, with the respective distributions $I_tL(\ln \tau)$ shown as insets. For this diblock, the static structure factor exhibits a maximum at a $\theta = 55°$ scattering angle corresponding to $q^* \approx 1.7 \times 10^{-2}$ nm^{-1}. It is evident that the most probable composition fluctuations, with length scale corresponding to the strong maximum of the scattering intensity at a finite wavevector q^* (note the different scales in the y-axes of the insets), relax significantly slower than those with both larger and smaller length scales (lower or higher wavevectors, respectively). The correlation function is dominated for all scattering angles by the slower of the three modes observed in the distribution of relaxation times (insets): (i) a very weak fast process (barely seen faster than $\sim 10^{-3}$ s), which is the cooperative diffusion discussed in relation to Figure 2 above (it is also clearly observed in the inset of Figure 3 at 1.26%); (ii) an intermediate process (also weak, which appears as concentration increases); and (iii) a dominant slower process (more than 97% of the total

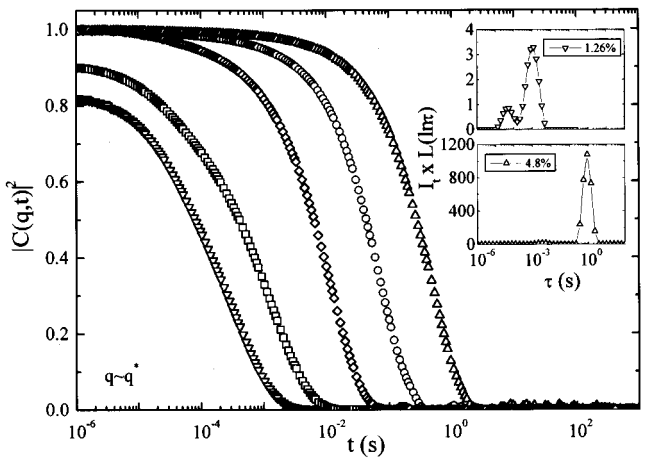

Figure 3. Net intensity autocorrelation functions $|C(q,t)|^2$ for toluene solutions of SI-2M50 at 20 °C for $q = 2.5 \times 10^{-2}$ nm$^{-1} \approx q^*$ and different copolymer concentrations: 1.26 (▽), 2.09 (□), 3.57 (◇), 3.86 (○), and 4.8 wt % (△). The insets show the respective distributions of relaxation times $L(\ln \tau)$ for the lower and the higher concentrations multiplied by the total scattering intensity reduced by that of toluene, I_t.

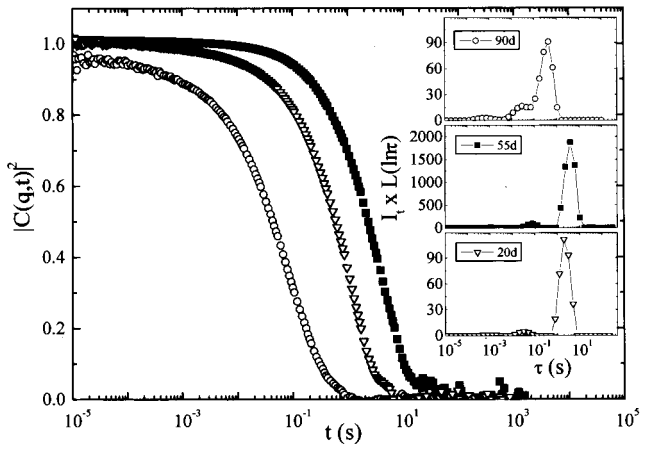

Figure 4. Net intensity autocorrelation functions for a 2.6 wt % SI-3M50 solution in toluene at 20 °C for scattering angles $\theta = 90°$ (○), 55° (■), and 20° (▽). The insets show the corresponding distributions of relaxation times $L(\ln \tau)$ multiplied by the total scattering intensity reduced by that of toluene, I_t.

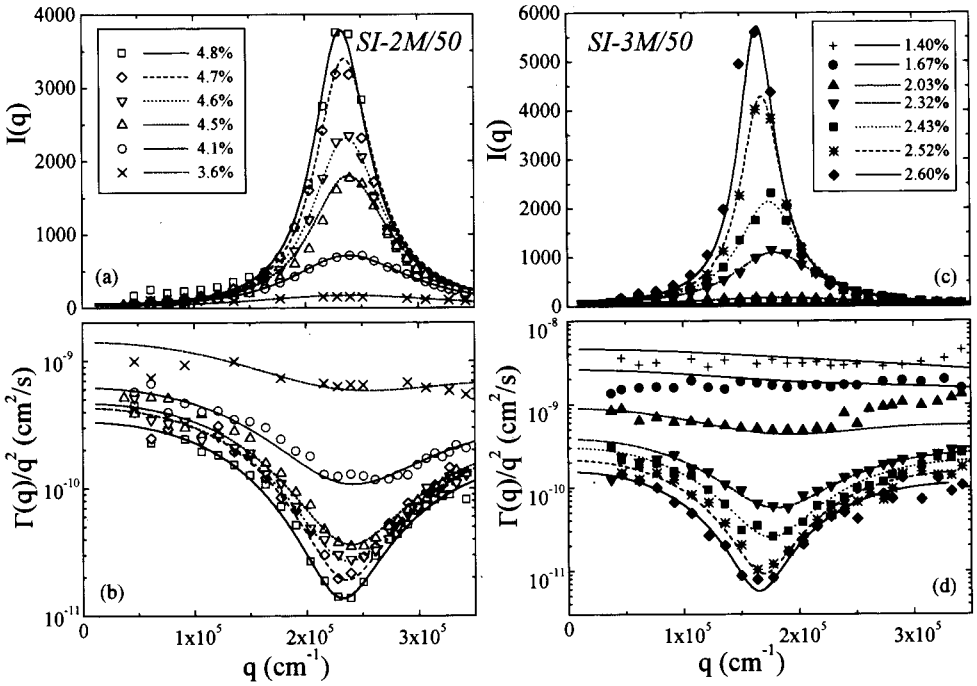

Figure 5. Wavevector dependence of the intensities $I(q)$ (a, c) and the effective diffusion coefficients $D(q) = \Gamma(q)/q^2$ (b, d) of the main relaxation mode for toluene solutions of SI-2M50 (a, b) and SI-3M50 (c, d) as a function of copolymer concentration (in the legends in wt %). The curves are the theoretical calculations based on eqs 13, 8, and 16.

intensity near q^* and at low angles and more than 70% at high angles). This dominant mode of relaxation of composition fluctuations is the focus of the present paper; the intermediate process is briefly discussed in Appendix B.

The intensities and the effective diffusion coefficients, $D(q) = \Gamma(q)/q^2$, are shown in Figure 5 for the dominant mode of relaxation of composition fluctuations as a function of wavevector and concentration for both SI-2M50 (Figure 5a,b) and SI-3M50 (Figure 5c,d). Increasing the thermodynamic incompatibility χ^*N (by increasing the concentration) toward ODT influences significantly not only the static scattering intensity but the relaxational dynamics as well. Linking together the two blocks in a diblock copolymer leads to a retardation (slowing down) of the dynamics both as a function of the wavevector and as a function of χ^*N. The relaxation of composition fluctuations over a finite length scale (finite wavevector), corresponding to the most probable composition fluctuations (responsible for the peak in $S(q)$ at q^*), is much slower than that for fluctuations over long length scales (low wavevectors). Moreover, as χ^*N increases, the dynamics over finite length scales exhibits a strong thermodynamic slowing down, which mirrors the significant intensity increase at q^*. It is, therefore, evident that the most probable composition fluctuations are long-lived even when they occur over finite length scales. These results demonstrate the difference between diblock copolymers and polymer blends: for intramolecular mixtures (copolymers) the slowing down occurs over finite length scales ($q \to q^*$) as the microphase separation is approached, whereas, for the usual intermolecular mixtures (blends), the slowing down of the dynamics takes place in the thermodynamic limit ($q \to 0$) as they approach the macrophase separation.[1]

Besides the behavior of the intensity and the effective diffusion coefficient of the main mode around q^*, which relates this process to the internal copolymer mode, it is important to examine their q dependencies for lower wavevectors ($q \ll q^*$), i.e., in a regime approaching the well-studied regime of $qR_g \ll 1$.[8−10,17] For all the concentrations investigated, the intensity of this mode tends to a constant at low wavevectors ($I(q \to 0) \to$ constant) as well as its effective diffusion coefficient $D(q \to 0) \equiv \Gamma(q \to 0)/q^2 \to$ constant; actually, this diffusion coefficient $D(q \to 0)$ is very close to the chain self-diffusion coefficient D_s measured independently with pulsed-field-gradient nuclear magnetic resonance.[28] Therefore, in the $q \ll q^*$ regime, the features of the mode observed are reminiscent of the polydispersity-induced self-diffusion process, although the characteristics near q^* and for higher χ^*N resemble those anticipated for the "internal" copolymer mode of monodisperse diblocks. To explain these features and identify the true character of the mode, a complete theory is developed for the relaxation of composition fluctuations for real polydisperse diblock copolymers over the whole wavevector regime; this is presented in section IV.

The strong increase of the intensity and the concurrent significant slowing down of the dynamics at q^* are demonstrated in the reduced representation of Figure 6. The reduced structure factor $\tilde{S}(q^*;\phi) = [I(q^*;\phi)/(N\phi)]\cdot F(u^*,f_A)$ is shown as a function of the reduced distance from the ODT expressed as $\epsilon(\phi) = [\chi^*_{ODT} - \chi^*]/\chi^*_{ODT} = [\phi_{ODT}^{1.59} - \phi^{1.59}]/\phi_{ODT}^{1.59}$. $F(u^*,f_A)$ is a characteristic constant[2,29] for a diblock with composition f_A and $u = q^2 R_g^2$ (u^* corresponds to q^*), which includes the effects of polydispersity of the static behavior.[29] The data for the two copolymers collapse onto the same master curve whereas the significant increase in the value of $\tilde{S}(q^*;\phi)$ by approaching the ODT is due to the increasing composition fluctuations with most probable wavelength $\sim 2\pi/q^*$. The same thermodynamic interactions are responsible for the almost 2 orders of magnitude suppression of the reduced effective diffusion coefficient $\tilde{D}(q^*;\phi) = D(q^*;\phi)/D_s(\phi)$, which is also plotted as a

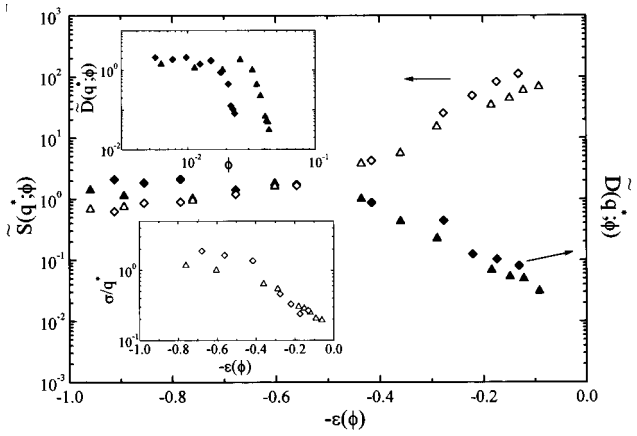

Figure 6. Reduced diffusion coefficient $\tilde{D}(q^*;\phi) = D(q^*;\phi)/D_s(\phi)$ (right axis) and the corresponding normalized (according to the mean-field theoretical prediction) structure factor $\tilde{S}(q^*;\phi)$ (left axis) for the most probable composition fluctuations with wavevector q^*, as a function of the reduced distance from the ODT, $\epsilon(\phi)$, in the neutral good solvent toluene at 20 °C. The chain self-diffusion coefficient $D_s(\phi)$ is obtained from the same dynamic light scattering experiments in the limit $q \to 0$ (see text). The upper inset shows the reduced diffusion coefficient $\tilde{D}(q^*;\phi)$ as a function of the polymer concentration, ϕ, whereas the lower inset shows the full width at half-maximum of the intensity peak, σ, reduced by the respective q^* vs the reduced distance from the ODT. (△, ▲): SI-2M50; (◇, ◆): SI-3M50.

function of the reduced distance from the microphase separation. The chain self-diffusion coefficient $D_s(\phi)$ was obtained from the same dynamic light scattering experiment in the limit of the lowest wavevectors, as discussed earlier. The upper inset of Figure 6 shows the same dynamic quantity $\tilde{D}(q^*;\phi)$ as a function of concentration ϕ, demonstrating that indeed the representation vs the reduced distance from the ODT expressed as $\epsilon(\phi)$ can eliminate the differences between the two diblocks. The reduced distance from the ODT can also allow superposition of the widths σ of the structure factor peaks (they become narrower by approaching the ODT) reduced by the peak position q^*, shown in the lower inset of Figure 6; σ is expressed as the full width at half-maximum of a Lorenzian function, which can represent the intensity data near the transition and is inversely proportional to the coherence length of the disordered structure. It is interesting to note that both the two static quantities, $\tilde{S}(q^*;\phi)$ and σ/q^*, and the dynamic quantity, $\tilde{D}(q^*;\phi)$, deviate from the behavior away from the transition (almost independent of $\epsilon(\phi)$) at about the same reduced concentration ($\epsilon \sim 0.5$), verifying the observation that it is the enhanced composition fluctuations which determine the dynamics; actually, the slowing down of $\tilde{D}(q^*;\phi)$ is evident when the composition fluctuations become sufficiently coherent as indicated by the value of the ratio $q^*/\sigma > 2$.

IV. Theoretical Approach

IV.1. The Diblock Copolymer System. The dynamic structure factor of a symmetric monodisperse diblock copolymer system ($N_A = N_B$) in the entanglement regime over the whole qR_g range[4,12] as well as the large-scale ($qR_g \ll 1$) behavior[9,16,17] of a polydisperse system have been investigated before. The aim of the present work is to calculate the dynamic structure factor in the general case of compositionally polydisperse entangled diblocks over the whole qR_g range. Two basic types of fluctuations are distinguished: (i) fluctuations of the total concentration $\phi = \phi_A + \phi_B$ and (ii) composition fluctuations characterized by the order parameter $\delta\phi_A$ (eq 1). The amplitude of total-concentration fluctuations[14] is usually negligible in experimentally interesting regimes (see section III) in comparison with that of composition fluctuations, which is the focus of the present work.

One may consider a polydisperse diblock copolymer consisting of geometrically similar blocks A and B (same statistical segment length, b, and volume per link v) with long enough chains, so that the system is entangled. A diblock copolymer chain can be characterized by two parameters: the total number of segments $N \equiv N_A + N_B$ and the composition parameter $f = (N_A - N_B)/(N_A + N_B)$. Here N_A and N_B are the number of segments of A and B blocks, respectively. If $\rho(f)$ is the volume fraction of molecules of kind f, the composition distribution function of copolymer molecules is $F(f) = \rho(f)/\phi$, where $\phi = \int_{-1}^{1}\rho(f)\,df$. The composition polydispersity is characterized by $\delta_f = \int_{-1}^{1} f^2 F(f)\,df - (\int_{-1}^{1} fF(f)\,df)^2$.

Compositionally symmetric diblock copolymers are, in principle, of specific interest since the microphase separation in this case occurs as a weakly first-order phase transition,[2] which means that the pretransitional order parameter fluctuations may be strong. Hence, the theory is developed for a *globally symmetric* diblock copolymer, which is monodisperse with respect to the total molecular weight (total N is constant independent of f) and for the case where the composition polydispersity is characterized by a symmetric composition distribution, $F(f) = F(-f)$. In this case, $\bar{\phi}_A = \bar{\phi}_B$ and $M_{w_A}/M_{n_A} - 1 = M_{w_B}/M_{n_B} - 1 = \delta_f$, where M_{w_i} and M_{n_i} are the weight-averaged and number-averaged molecular weights of the i-block, respectively. A particular case of such a system is a bidisperse *symmetric* mixture of diblock copolymers of two kinds:

$$N_A^{(1)} + N_B^{(1)} = N_A^{(2)} + N_B^{(2)} = N; \quad N_A^{(1)} = N_B^{(2)}; \quad N_B^{(1)} = N_A^{(2)} \tag{5a}$$

$$F(f) = [\delta(f - f') + \delta(f + f')]/2; \quad f' = \frac{N_A^{(1)} - N_B^{(1)}}{N}; \quad \delta_f = [f']^2 \tag{5b}$$

The usefulness of this bidisperse system in the analysis for the dynamic structure factor of a polydisperse system will become evident later.

IV.2. The Dynamic Random Phase Approximation Approach. The dynamic structure factor $S_{ij}(\mathbf{q},t)$ of a system consisting of polymer molecules formed of chemically different monomers is defined as

$$S_{ij}(\mathbf{q},t) = \frac{1}{v}\int \langle \delta\phi_i(0,0)\,\delta\phi_j(\mathbf{r},t)\rangle \exp[-i\mathbf{q}\cdot\mathbf{r}]\,d\mathbf{r} \tag{6}$$

where $\delta\phi_j(\mathbf{r},t) = \phi_j(\mathbf{r},t) - \bar{\phi}_j$ is the deviation of the volume concentration of the jth component from its equilibrium value. For isotropic systems, $S_{ij}(\mathbf{q},t) = S_{ij}(q,t)$. The fluctuation−dissipation theorem[30] relates the dynamic structure factor with the matrix of generalized linear susceptibilities $\kappa_{ij}(q,t)$; for a system obeying classical statistics,

$$\kappa_{ij}(q,t) = -H(t)\frac{\partial S_{ij}(q,t)}{\partial t} \tag{7a}$$

$$\kappa_{ij}(q,p) = S_{ij}(q,t)|_{t=0} - pS_{ij}(q,p) \tag{7b}$$

where $H(t)$ is the Heaviside function and the Laplace transform $g(p) = \int_0^\infty g(t)\exp(-pt)\,dt$ is used. The linear susceptibility and the dynamic structure factor are calculated using the dynamic random phase approximation[31,4] (RPA) approach utilizing the susceptibilities of an "ideal polymer system", in which the intermonomer interactions are switched off, $\kappa_{ij}^{(0)}(q,p)$. As has been shown[4] in the framework of the Flory−Huggins model for a two-component (A → 1, B → 2) incompressible ($\phi_A + \phi_B$ = constant) copolymer,

$$\kappa_{ij}(q,p) = \kappa(q,p)(2\delta_{ij} - 1) \tag{8a}$$

$$\frac{1}{\kappa(q,p)} = \frac{1}{\kappa^{(0)}(q,p)} - 2\chi \tag{8b}$$

$$\kappa^{(0)}(q,p) = \frac{\kappa_{11}^{(0)}\kappa_{22}^{(0)} - (\kappa_{12}^{(0)})^2}{\kappa_{11}^{(0)} + 2\kappa_{12}^{(0)} + \kappa_{22}^{(0)}} \tag{8c}$$

where δ_{ij} is the Kronecker delta.

For a compositionally polydisperse copolymer, $\kappa_{ij}^{(0)}(q,p)$ can be written as

$$\kappa_{ij}^{(0)}(q,p) = \int_{-1}^{1}\kappa_{ij}^{(0,f)}(q,p)\,\rho(f)\,df \tag{9}$$

where $\kappa_{ij}^{(0,f)}(q,p)$ is the susceptibility of a diblock copolymer of a kind f and $\rho(f) = \phi F(f)$. Note that $\kappa_{11}^{(0,f)} = \kappa_{22}^{(0,-f)}$ and $\kappa_{12}^{(0,f)} = \kappa_{21}^{(0,-f)} = \kappa_{12}^{(0,-f)}$. Hence, for a symmetric composition distribution function $F(f) = F(-f)$ assumed in section IV.1, the relation $\kappa_{11}^{(0)}(q,p) = \kappa_{22}^{(0)}(q,p)$ is satisfied. This allows a simplification of eq 8c as

$$\kappa^{(0)}(q,p) = \frac{\phi}{2}\int_{-1}^{1}\{\kappa_{11}^{(0,f)}(q,p) - \kappa_{12}^{(0,f)}(q,p)\}F(f)\,df \tag{10}$$

In most cases, the dynamic structure factor, $S(q,t) \equiv S_{11}(q,t)$ (see eq 2), of an equilibrium homogeneous system can be written as a superposition of relaxation modes

$$S(q,t) = \sum_k I_k(q)\exp[-\Gamma_k(q)t] \tag{11}$$

$I_k(q)$ is the intensity of the kth mode and $\Gamma_k(q)$ its relaxation rate. In this case, the linear susceptibility $\kappa(q,p) \equiv \kappa_{11}(q,p)$ is a meromorphic function (all singularities are poles), and all poles are simple and located in half-plane Re(p) < 0:

$$\kappa(q,p) = \sum_k \frac{I_k(q)\,\Gamma_k(q)}{p + \Gamma_k(q)} \tag{12}$$

Therefore, the set of relaxation rates and intensities can be evaluated with

$$1/\kappa(q,-\Gamma_k) = 0; \quad I_k = \frac{1}{\Gamma_k}\mathrm{Res}_{p=-\Gamma_k}[\kappa(q,p)] \tag{13}$$

where Res means the residue of a pole singularity (in the above equation, $I_k = I_k(q)$ and $\Gamma_k = \Gamma_k(q)$). The log-

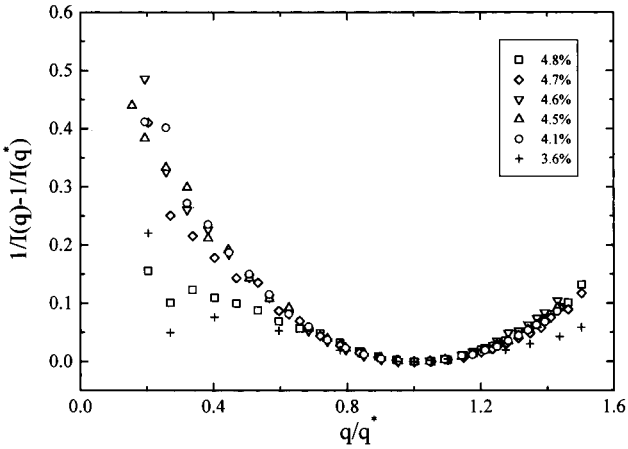

Figure 7. Reduced plot of $1/I(q) - 1/I(q^*)$ vs $\tilde{q} = q/q^*$ for the SI-2M50 toluene solutions (see text).

averaged relaxation rate $\bar{\Gamma}(q)$, which may be used to characterize the dynamics (if the various modes are not resolved), is

$$\bar{\Gamma}(q) = \exp(\sum_k I_k(q)\ln[\Gamma_k(q)]/I_{\text{total}}) \tag{14a}$$

where $I_{\text{total}} = \sum_k I_k(q) \equiv \kappa(q,0)$. Using eqs 7 and 11−13, one gets

$$\bar{\Gamma}(q) = \exp\left\{\int_0^1\left[\frac{\kappa(q,p) + \kappa(q,p^{-1})}{\kappa(q,0)} - 1\right]\frac{dp}{p}\right\} \tag{14b}$$

The above theoretical results are directly applicable to an incompressible copolymer melt. In the case of the solutions used in the present work, the total polymer concentration $\phi = \phi_A + \phi_B$ may also fluctuate. However, since, as discussed earlier, the concentration fluctuations are much weaker than the composition fluctuations, the system in this respect can be considered as incompressible. Moreover, in semidilute solutions the interaction parameter χ should be renormalized[9,20,23] as $\chi^* \cong \chi\phi^{1.59}$. This allows application of the theoretical results for both block copolymer melts and semidilute solutions.

Setting $p = 0$ in eq 8b and using eq 7, one obtains $1/S(q) = 1/S^{(0)}(q) - 2\chi^*$, where $S(q) \equiv S_{11}(q)$. Hence, the curves $1/S(q)$ vs q measured for different values of χ^* should superimpose by an appropriate vertical shift. An attempt to verify this is shown in Figure 7 using the dynamic light scattering intensity data, $I(q) \propto S(q)$, of the toluene solutions of SI-2M/50 for different concentrations in the disordered state. In Figure 7, the wavevector (x-axis) is shown as $q/q^* = \tilde{q}$, i.e., reduced by q^* that corresponds to the maximum of $I(q)$, whereas the quantity $1/I(q) - 1/I(q^*)$ is scaled in order to satisfy the relation $(\partial^2[I(\tilde{q})]^{-1}/\partial\tilde{q}^2)|_{\tilde{q}=1} = 1$, this scaling is performed in order to eliminate the concentration dependence. The reasonable superposition of the data (except for the lowest and the highest concentrations at low wavevectors) verifies the validity of the RPA.

The above eqs 8−14 may be utilized to calculate the dynamic structure factor $S(q,t)$ and its relaxation processes for an interactive polydisperse system provided that $\kappa_{ij}^{(0,f)}(q,p)$ in eq 9 is known. Its derivation for an ideal system requires a motional mechanism for the entangled copolymer chains, which is provided by the classical reptation model.[26] The calculations for the

probability distribution functions and for the susceptibility components of a diblock copolymer of type *f*, $\kappa_{ij}^{(0,f)}(q,p)$, are presented in Appendix A.

The susceptibility of a polydisperse system can be calculated utilizing the ideal bidisperse system (defined in section IV.1), whose susceptibility, $\kappa_{\rm bi}^{(0)}(q,p)$, is calculated in Appendix A (eq A8). Thus,

$$\kappa_{\rm poly}^{(0)}(q,p) = \int_{-1}^{1} \kappa_{\rm bi}^{(0)}(q,p)\, F(f')\, {\rm d}f' \qquad (15)$$

The simplest symmetric distribution function is a steplike distribution $F(f') = 0$ for $|f'| > (\delta f)$ and $F(f') = [2(\delta f)]^{-1}$ for $|f'| < (\delta f)$. In this case, the susceptibility of an "ideal" polydisperse system is given by

$$\kappa_{\rm poly}^{(0)}(q,p) = \frac{1}{2(\delta f)} \int_{-(\delta f)}^{(\delta f)} \kappa_{\rm bi}^{(0)}(q,p)\, {\rm d}f' = \frac{\phi N u}{(\delta f)(u^2-\sigma^2)} \left\{ \Psi_2(u) - \Psi_2(\sigma) + \frac{\sinh[(\delta f)\sigma] - (\delta f)\sigma}{\sigma^2[{\rm e}^{\sigma}(u+\sigma)/(u-\sigma)+1]} + \frac{(\delta f)\sigma(\cosh\sigma + 2) + \sinh[(\delta f)\sigma] - 8\cosh(\sigma/2)\sinh[(\delta f)\sigma/2]}{\sigma^2[{\rm e}^{\sigma}(u+\sigma)/(u-\sigma)-1]} \right\} \qquad (16)$$

where

$$\Psi_2(x) = [4{\rm e}^{-x[(\delta f)+1]/2}({\rm e}^{x(\delta f)} - 1) - x(\delta f)({\rm e}^{-x} + 3)]/(2x^2)$$

The polydispersity parameters f' for the bidisperse distribution and δf for the steplike distribution are related with the usual polydispersity degree $M_{\rm w_A}/M_{\rm n_A}$ of one block as

$$\delta_f = \frac{M_{\rm w_A}}{M_{\rm n_A}} - 1 = (f')^2 \qquad \text{bidisperse case} \quad (17a)$$

$$\delta_f = \frac{M_{\rm w_A}}{M_{\rm n_A}} - 1 = \frac{(\delta f)^2}{3} \qquad \text{polydisperse case} \quad (17b)$$

Equations 8b and 16 allow the calculation of the response functions for the symmetric polydisperse diblock copolymers. If $\kappa(q,p)$ is an analytical function of p for ${\rm Re}(p) < 0$, one can numerically evaluate the dynamic structure factor by finding the poles and residues of $\kappa(q,p)$ as a function of χ^* for each δf utilizing eqs 11−13. All poles are situated at the real axis at ${\rm Re}(p) < 0$ if $\chi^* < \chi_{\rm s}^*(\delta f)$, where

$$N\chi_{\rm s}^*(\delta f) = \frac{1}{2\kappa^{(0)}(q^*,p=0)} \qquad (18)$$

where q^* is a value corresponding to the maximum of $\kappa^{(0)}(q,p=0)$. It is noted that both $Q^* = q^*R_{\rm g} = q^*N^{1/2}b/\sqrt{6}$ and $N\chi_{\rm s}^*(\delta f)$ vary with the polydispersity degree from $Q^* \cong 1.95$ and $N\chi_{\rm s}^*(\delta f) \cong 10.5$ at $\delta f = 0$ to $Q^* \cong 1.3$ and $N\chi_{\rm s}^*(\delta f) \cong 8.0$ at $\delta f = 0.8$, in agreement with earlier calculations[29,32] for the static structure factor. Moreover, $Q^* \to 0$ and $N\chi_{\rm s}^*(\delta f) \to 6$, for $\delta f \to 1$. A singularity of $\kappa(q,p)$ at a positive p means that the homogeneous state of the system, with the equilibrium structure factor $S(\mathbf{r},\mathbf{r}',t) = S(\mathbf{r}-\mathbf{r}',t)$, becomes unstable, and the components of the system will undergo a micro-or/and macrophase separation.

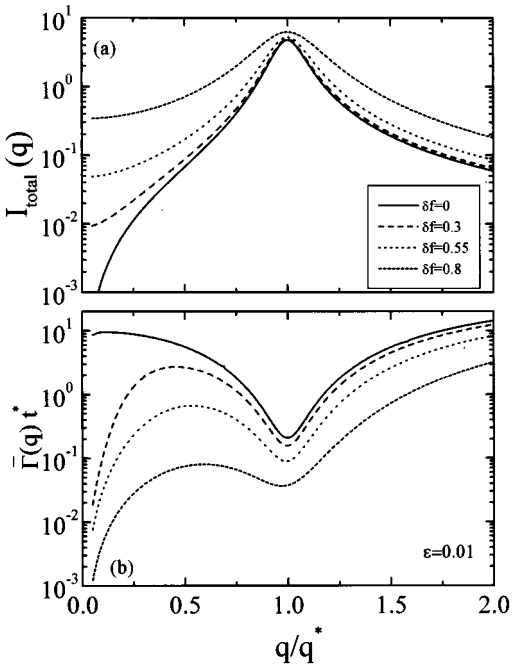

Figure 8. Theoretical predictions for the wavevector dependence of (a) the total intensity $I_{\rm total}(q)$ and (b) the log-average dimensionless relaxation rate $\bar{\Gamma}(q)t^*$ vs $\tilde{q} = q/q^*$ for polydisperse diblock copolymers with various degrees of polydispersities δf at the same reduced distance from the ODT $\epsilon = 0.01$.

IV.3. Influence of Compositional Polydispersity. One can now use eqs 8, 13, and 16 to calculate the scattering intensities, $I_k(q)$, and relaxation rates, $\Gamma_k(q)$, for the various modes $k = 1, 2, \ldots$, as well as the total scattering intensity $I_{\rm total}(q) = S(q)$ and the log-averaged relaxation rate $\bar{\Gamma}(q)$ (eq 14). The calculations are performed for a polydisperse system with the steplike polydispersity distribution as a function of the degree of polydispersity and the interaction parameter.

Before proceeding with demonstrating the numerical results for the various relaxation modes, one may discuss certain qualitative features of the theory presented herein. Figure 8 shows the dependence of the total scattering intensity, $I_{\rm total}(q) = S(q)$ (Figure 8a), and the respective log-averaged relaxation rate, $\bar{\Gamma}(q)$ (Figure 8b), as a function of the reduced wavevector q/q^* for different values of the composition polydispersity parameter δf, assuming the steplike polydispersity distribution function, and for the same relative distance from the critical point for microphase separation expressed with the parameter $\epsilon = [\chi_{\rm s}^*(\delta f) - \chi^*]/\chi_{\rm s}^*(\delta f) = 0.01$. Significant changes with the degree of composition polydispersity are evident in both the intensity and the effective relaxation rate. The static intensity calculations qualitatively agree with earlier works; in the present work only the composition polydispersity was introduced whereas, in previous studies,[29,32] either only molecular weight polydispersity was assumed or both molecular weight and composition polydispersity. Composition polydispersity increases the scattering intensity at low wavevectors with the intensity tending to a finite value as $q \to 0$; this value increases with increasing δf. The shift in the position of the maximum q^* to lower wavevectors by increasing δf is not demonstrated in the present figure since the x-axis is shown in a reduced form $\tilde{q} = q/q^*$. The effect of δf on the log-averaged relaxation rate $\bar{\Gamma}(q)$ is more interesting within the present work. For $\delta f \to 0$, $\bar{\Gamma}(q)$ tends to a constant as q

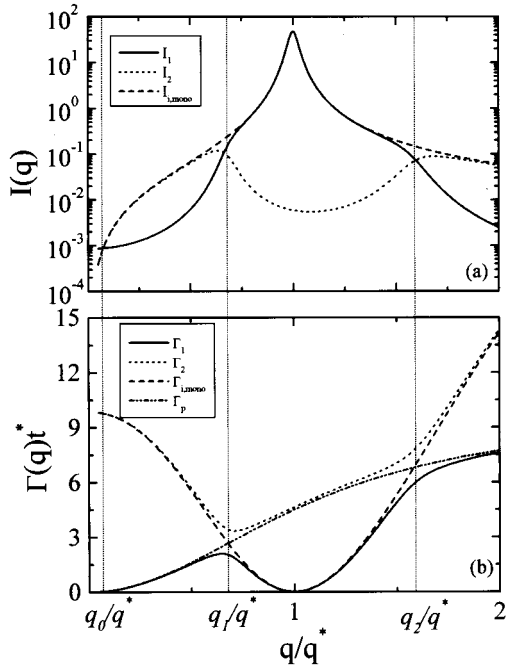

Figure 9. Theoretical predictions for the wavevector dependence of (a) the intensities $I(q)$ and (b) the dimensionless relaxation rates $\Gamma(q)t^*$ for a monodisperse diblock ($I_{i,\mathrm{mono}}(q)$, $\Gamma_{i,\mathrm{mono}}(q)$, dashed lines), the main "polydispersity" mode of eq 19 in the limit $\delta f \to 0$ ($\Gamma_p(q)$, dash−dot−dot−dash lines), and the two slower modes ($k = 1, 2$) for a polydisperse diblock with low $\delta f = 0.1$: ($I_1(q)$, $\Gamma_1(q)$, solid lines) and ($I_2(q)$, $\Gamma_2(q)$, dotted lines). The calculations are shown for $\epsilon = 0.001$. The thin vertical lines denote the three characteristic wavevectors q_0, q_1, and q_2 (see text).

$\to 0$, in agreement with the behavior of the "internal" mode discussed before.[7−13] However, as δf increases, $\bar{\Gamma}(q) \to 0$ as $q \to 0$; actually with increasing δf, $\bar{\Gamma}(q)/q^2 \to$ constant (not shown in Figure 8; it will be discussed later), thus exhibiting a behavior reminiscent that of the so-called "polydispersity" mode.[8−10,13,16,17]

One can now proceed to the discussion of the behavior of the predicted relaxation modes ($k = 1, 2, ...$) and put them into perspective. An analysis has been presented previously[12] on the dynamic structure factor for monodisperse diblock copolymers within the reptation model. That analysis resulted in a set of reptational modes with only the slowest one having significant intensity to be experimentally observed. The relaxation rate of that process $\Gamma_{i,\mathrm{mono}}(q)$ is shown in Figure 9 (dashed line) for $\epsilon = 0.001$. A polydisperse system is characterized by extra relaxation modes that are due to composition polydispersity. An analysis of eq 16 at the limit of very weak polydispersity, $\delta f \to 0$, shows that the intensity of these extra modes is proportional to $(\delta f)^2$, and their relaxation rates are given by the equation

$$\frac{Q^2}{\sqrt{\Gamma t^*}} = \tan(\sqrt{\Gamma t^*}/2) \quad \text{or}$$

$$\frac{\sqrt{\Gamma t^*}}{2} = \arctan\left(\frac{Q^2}{\sqrt{\Gamma t^*}}\right) + \pi l, \quad l = 0, 1, 2, ... \quad (19)$$

where $Q \equiv qR_g$ and t^* is proportional to the disentanglement time $t_d = t^*/\pi^2$ (Appendix A). The relaxation rate $\Gamma_p(q)$ of the main "polydispersity" mode (with $l = 0$) is shown in Figure 9b as the dash−dot−dot−dash line ($\Gamma_p(q)$ does not depend on χ in the limit $\delta f \to 0$). Higher-order "polydispersity" modes (with $l > 0$) can be neglected as their intensities are very low. Note that the two curves $\Gamma_p(q)$ and $\Gamma_{i,\mathrm{mono}}(q)$ intersect each other at two wavevectors: $q = q_1$ and $q = q_2$. For a small, but finite, degree of polydispersity (for example, $\delta f = 0.1$ in Figure 9), these two modes are transformed into the slowest ($k = 1$) and the next higher-order ($k = 2$) mode of the real polydisperse system. Their relaxation rates $\Gamma_1(q)$ and $\Gamma_2(q)$ are shown in Figure 9 as solid and dotted lines, respectively. Note that always $\Gamma_1(q) < \Gamma_2(q)$ due to eigenvalue repulsion; i.e., the corresponding curves do not intersect each other. The first (the slowest) mode is almost identical to the polydispersity one ($\Gamma_1(q) \cong \Gamma_p(q)$) for $q < q_1$ and $q > q_2$ (it is due to polydispersity). However, it nearly coincides with the internal mode of the monodisperse system ($\Gamma_1(q) \cong \Gamma_{i,\mathrm{mono}}(q)$) for $q_1 < q < q_2$. Similarly, the second mode (the faster) is almost identical to the internal mode ($\Gamma_2(q) \cong \Gamma_{i,\mathrm{mono}}(q)$) for $q < q_1$ and $q > q_2$, whereas it coincides with the polydispersity one ($\Gamma_2(q) \cong \Gamma_p(q)$) for $q_1 < q < q_2$; i.e., the second mode is due to polydispersity in this regime. Besides, low intensity is calculated for the first (slowest) mode for $q < q_1$ and $q > q_2$ (in the case of weak polydispersity), as well as for the second (faster) mode for $q_1 < q < q_2$ (Figure 9). Therefore, it is the second mode that dominates for wavevectors just below q_1. However, as q decreases further, the intensity of the second mode decreases, and it tends to go to zero as $q \to 0$ following the behavior of the internal mode of a monodisperse system. So $I_2(q)$ becomes lower than $I_1(q)$ for small wavevectors, $q < q_0$ (note that $I_1(q)$ does not vanish in the limit $q \to 0$). Thus, one can account for the three intersections between the intensities curves, $I_1(q)$ and $I_2(q)$, at q_0 and near q_1 and q_2. It is noted that the intensity of the second mode shows two maxima near q_1 and q_2. For $q < q_1$, its intensity increases with increasing q, since it is identical to the internal mode of a monodisperse system. However, for $q > q_1$ the mode is due to the (low) polydispersity, and thus, its intensity should be low. Therefore, it exhibits a maximum in the vicinity of q_1. Similar arguments may explain the second maximum in the vicinity of q_2.

One can calculate the relaxation rate and intensity of the slowest mode for the polydisperse system in the limit $q \to 0$:

$$\frac{\Gamma_1(q)t^*}{Q^2} \cong \left(2 - \frac{(\delta f)^2\chi^*N}{3}\right) - Q^2\left(\frac{1}{3} + (\delta f)^2\chi^*N \times \frac{15(\chi^*N + 4) - 2(\delta f)^2(5\chi^*N + 9) + 3(\delta f)^4\chi^{*2}N}{540}\right) + O(Q^4) \quad (20a)$$

$$I_1(q) \cong \frac{\phi N(\delta f)^2}{12[1 - (\delta f)^2\chi^*N/6]}\{1 + Q^2[180(6 - (\delta f)^2\chi^*N)]^{-1}[180(\chi^*N - 1) - 3(\delta f)^2(36 + 40\chi^*N + 5(\chi^*N)^2) + 2(\delta f)^4\chi^*N(18 + 5\chi^*N) - 3(\delta f)^6(\chi^*N)^2]\} \quad (20b)$$

A few comments are in order. First, this mode is exclusively due to the composition polydispersity: its intensity is identically zero for a monodisperse system with $\delta f = 0$. Second, for $Q \equiv qR_g \ll 1$, its relaxation rate is proportional to Q^2 and its intensity is independent of

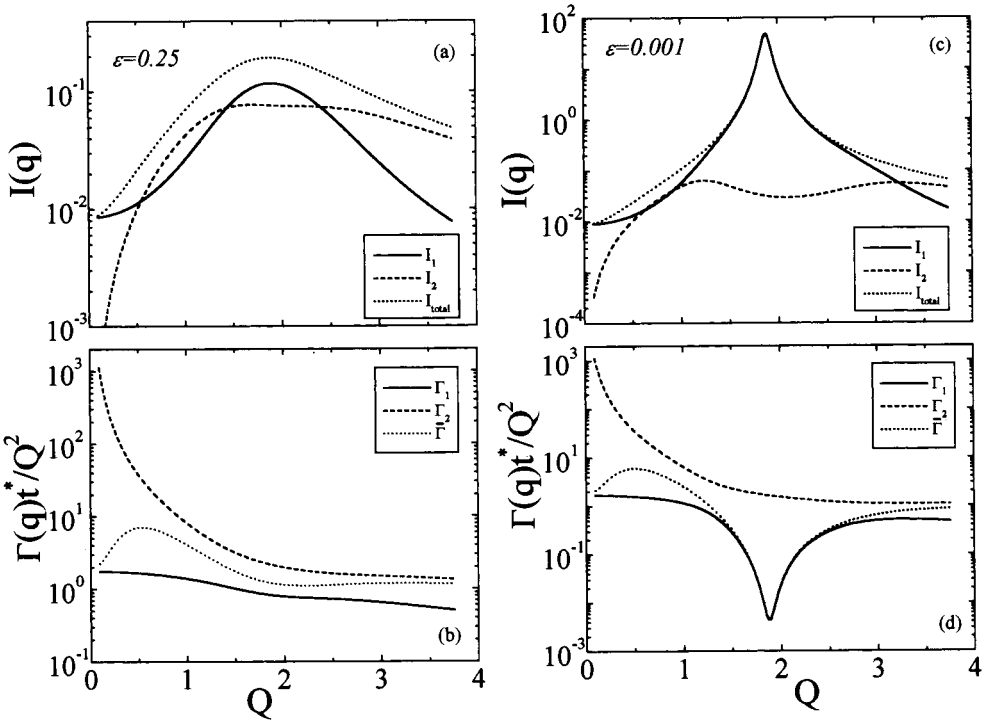

Figure 10. Theoretical predictions for the intensities $I_k(q)$ (a, c) and reduced diffusion coefficients $\Gamma_k(q)t^*/Q^2$ (b, d) of the two slower modes with $k = 1$ (solid lines) and $k = 2$ (dashed lines), the total intensity (dotted lines in a, c), and the mean reduced diffusion coefficient $\bar{\Gamma}(q)t^*/Q^2$ (dotted lines in b, d) for a polydisperse diblock with $\delta f = 0.3$ as a function of the wavevector $Q = qR_g$ for two different reduced distances from the ordering transition $\epsilon = 0.25$ (a, b) and $\epsilon = 0.001$ (c, d).

Q and tends to a constant as $Q \to 0$; this constant is proportional to the degree of composition polydispersity $(\delta f)^2$. Therefore, this process is diffusive with diffusion coefficient $D = \Gamma_1(q)/q^2 \cong (2 - (\delta f)^2\chi^*N/3)R_g^2/t^* = D_s(1 - (\delta f)^2\chi^*N/6)$, where $D_s = 2R_g^2/t^*$ is the self-diffusion constant within the reptation model. Therefore, this mode is indeed the "polydispersity" mode due to the interdiffusion of copolymer molecules of different composition, as investigated both experimentally and theoretically earlier.[8−10,13,16,17] Note that for a symmetric copolymer the parameter κ_0 used previously[10,16,17] to characterize the variance of the composition polydispersity is related to $(\delta f)^2$ by $\kappa_0 = (\delta f)^2/12$. The second mode nearly coincides with the internal mode of a monodisperse system for $Q \to 0$; its rate and intensity for $q \ll q^*$ are given by

$$\Gamma_2(q) \cong \pi^2/t^*; \quad I_2(q) \cong \phi N Q^2/24 \tag{21}$$

in agreement with earlier estimates.

IV.4. Pretransition Dynamics: Relaxation Modes. One can now study the behavior of the various modes of relaxation of composition fluctuations over the whole wavevector range. Figures 10 and 11 show the theoretical results for the dynamic intensities, $I_1(q)$ and $I_2(q)$, and the respective relaxation rates, $\Gamma_1(q)$ and $\Gamma_2(q)$, for the first two modes ($k = 1$, 2) obtained from the calculated susceptibility for two different degrees of polydispersity $\delta f = 0.3$ (Figure 10), corresponding to $M_w/M_n = 1.03$ usually encountered in ordinary molecular weight diblock copolymers,[8−10] and $\delta f = 0.8$ (Figure 11), corresponding to $M_w/M_n = 1.21$ larger than the one measured for the present ultrahigh molecular weight systems. In both figures the calculations are shown for two different distances from the critical point for microphase separation, i.e., for $\epsilon = 0.25$ (parts a and b) and $\epsilon = 0.001$ (parts c and d). The data for the relaxation rates are shown in the form of a reduced effective diffusion coefficient $\Gamma_k(q)t^*/Q^2 = 2D(q)/D_s$, where $D(q) = \Gamma_k(q)/q^2$.

For low δf and away for the transition (high ϵ), the modes show the behavior similar to that shown in Figure 9 and discussed above. For low $Q \equiv qR_g$, the two modes exhibit the characteristics observed previously[8−10,13,16,17] and identified with the "polydispersity" ($k = 1$) mode (exhibiting $\Gamma_1 \propto q^2$ and $I_1 \propto q^0$) and with the "internal" ($k = 2$) mode (with $\Gamma_2 \propto q^0$ and $I_2 \propto q^2$). This picture for low Q's is the same for every δf both far and near the transition; the differences observed are with respect to the relative intensities of the two processes as well as with respect to the range of low Q's, for which these observations hold. For higher Q's, however, the picture is more complicated. For low δf (Figure 10), the rate $\Gamma_1(q)$ of the slower mode is now a combined result of both internal (breathing) copolymer motions and copolymer interdiffusion. In the lower wavevector side, it is a continuation of the interdiffusion (polydispersity) process whereas for length scales of the order of the characteristic dimension of the structure, i.e., for $q \sim q^*$, it behaves similarly to an internal relaxation (of a monodisperse system) exhibiting a sharp increase of its intensity (which now dominates) together with a dramatic slowing down of its dynamics (the critical retardation) by approaching the ODT. The intensity of the second mode, $I_2(q)$, shows two maxima near $q = q_1$ and $q = q_2$ (see the discussion with respect to Figure 9). The effective diffusion coefficient corresponding to the mean relaxation rate, $\bar{\Gamma}(q)t^*/Q^2$, exhibits a nonmonotonic behavior: it increases as q increases in the low-q regime (due to the increasing intensity of the faster internal-like mode), and then it decreases as q approaches q^*, whereas it increases again for $q > q^*$.[33]

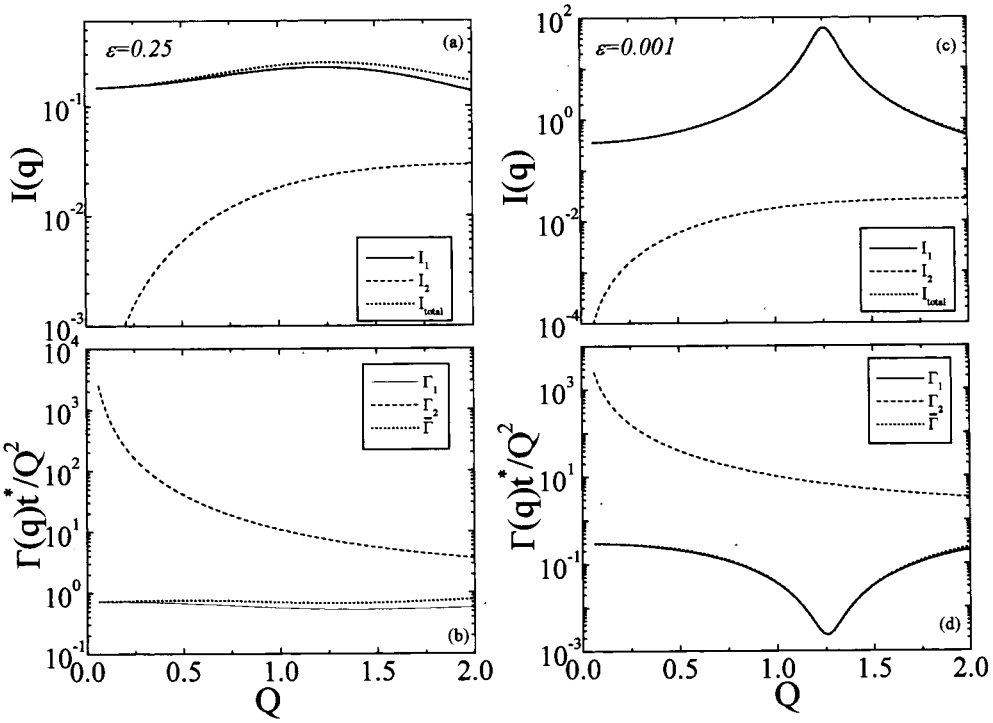

Figure 11. Theoretical predictions for the intensities $I_k(q)$ (a, c) and reduced diffusion coefficients $\Gamma_k(q)t^*/Q^2$ (b, d) of the two slower modes with $k = 1$ (solid lines) and $k = 2$, the total intensity (dotted lines in a, c), and the mean reduced diffusion coefficient $\bar{\Gamma}(q)t^*/Q^2$ (dotted lines in b, d) for a polydisperse diblock with $\delta f = 0.8$ as a function of the wavevector $Q = qR_g$ for two different reduced distances from the ordering transition $\epsilon = 0.25$ (a, b) and $\epsilon = 0.001$ (c, d).

For high δf, the slowest mode dominates over all others modes: $I_1(q) \gg I_2(q)$ in a wide range of q's (Figure 11) whereas the mean relaxation rate is essentially that of the slowest mode (except for very high Q's). The dominant mode exhibits characteristics similar to the experimental observations (Figure 5); i.e., at low wavevectors it is diffusive (reminiscent of the interdiffusion mode) whereas near q^* the behavior is similar to that anticipated for the internal mode with the critical retardation observed near the ODT (for low ϵ). In this δf regime, the theoretical results demonstrate that it is very difficult to experimentally resolve the second mode since its intensity is about 2 orders of magnitude smaller than that of the first slowest mode over the whole wavevector range. Note that this "high" polydispersity regime actually corresponds to ratios $M_w/M_n \geq 1.1$, which are still typical for synthetic polymers.

V. Discussion

The results of the theoretical analysis can be compared with the experimental dynamic light scattering data (intensities and relaxation rates, Figure 5) as a function of copolymer concentration in the solution as the ODT is approached; the systems in the present study are nearly symmetric diblocks, and thus, the theory for symmetric systems can be applied. The parameters involved in the comparison are the interaction parameter $\chi^*(\phi)$ (or equivalently the relative distance from the ODT, $\epsilon(\phi)$), the radius of gyration of the chain $R_g(\phi)$ (or equivalently the value of $Q^*(\phi)$), the characteristic time $t^*(\phi)$, and a proportionality constant K multiplier of the intensity (this should be independent of concentration). For the composition polydispersity parameter δf, the experimental values of M_w/M_n are used (Table 1) together with eq 17 for the polydisperse system.

The theoretical predictions for both the intensities $I_1(q)$ and relaxation rates $\Gamma_1(q)$ of the dominant slowest mode are shown in Figure 5 for both diblock copolymers SI-2M/50 and SI-3M/50 for all concentrations (see legends). An excellent agreement between the theory and the experiment is evident. The values of the polydispersity indices δf are 0.6 and 0.73 for copolymers SI-2M/50 and SI-3M/50, respectively, thus placing the systems in the "high"-polydispersity regime discussed with respect to Figure 11. The dominant mode ($k = 1$) for all concentrations shows the following behavior as the concentrations approach that for microphase separation transition, i.e., for low ϵ. For low wavevectors ($q \rightarrow 0$), its intensity $I_1(q)$ tends to a constant whereas its relaxation rate $\Gamma_1(q)$ is proportional to q^2 ($D(q) = \Gamma_1(q)/q^2 \rightarrow$ constant in Figure 5); i.e., it is essentially a diffusive process, similar to the polydispersity mode. As the wavevector increases, the intensity increases and the effective diffusion constant $D(q)$ decreases. $D(q)$ exhibits a critical retardation, and $I_1(q)$ shows a maximum for $q \cong q^*$; i.e., in this wavevector regime, the features are typical for those of the internal mode of a monodisperse system.

It is important to discuss the concentration dependence of the parameters utilized in the theoretical calculations (Figure 12). The intensity parameter K is independent of concentration, as it should, since it is only related to the optical setup, the incident beam, and the refractive index contrast between the two blocks. The interaction parameter $\chi^*(\phi)$ (Figure 12a) increases linearly with $\phi^{1.59}$ for concentrations not very near the transition (in agreement with the renormalization[21,24] in semidilute solutions in a nonselective good solvent) whereas it deviates toward smaller values near the transition; this is because fluctuation correction effects have not been introduced in the present theory.[2b,c] From

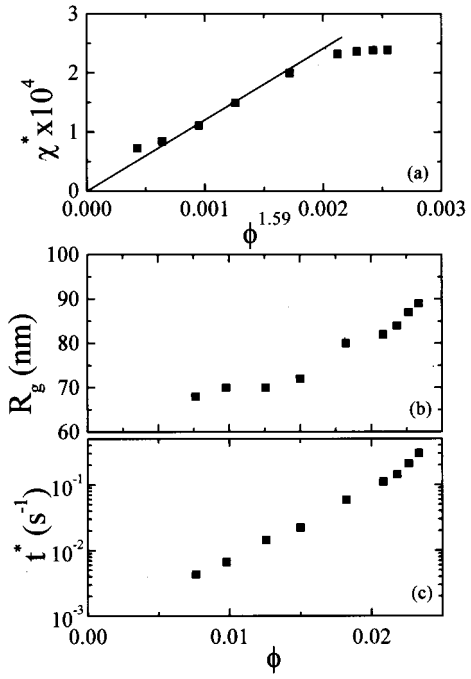

Figure 12. Estimated parameters from fitting the data in Figure 5 for toluene solutions of SI-3M50 at 20 °C with the theory described by eqs 13, 8, and 16: (a) the effective interaction parameter χ^* vs $\phi^{1.59}$ (the renormalization prediction); (b) the radius of gyration $R_g(\phi)$ vs concentration ϕ; (c) the characteristic time t^* vs concentration ϕ.

the slope of the $\chi^*(\phi)$ vs $\phi^{1.59}$ line, one can estimate the bare interaction parameter between polystyrene and polyisoprene as $\chi = 0.06-0.10$ (for SI-2M50 and SI-3M50, respectively), in agreement with earlier studies. The radius of gyration $R_g(\phi)$ (Figure 12b) shows a very weak dependence (if any) on ϕ for concentrations away from the transition (which conforms with the predicted $\phi^{-0.12}$ behavior in semidilute homopolymer solutions), whereas it increases near the transition, possibly due to chain extension as the ODT is approached.[2c] Finally, $t^*(\phi)$ (Figure 12c) increases with increasing ϕ much faster than the prediction ($\phi^{1.6}$) for the disentanglement time of entangled homopolymers; this should be due to thermodynamic effects influencing the longest relaxation time similarly to their influence on the self-diffusion coefficient.[28,35] Note that the self-diffusion coefficients estimated ($D_s = 2R_g^2/t^*$) using the values of Figure 2b,c are very close to those measured experimentally.[28]

Therefore, the theoretical analysis presented in section IV is capable of reproducing the experimentally observed behavior both qualitatively and quantitatively. An apparent contradiction may seem to be the fact that in the present paper the one dominant mode is mostly discussed while the theory predicts an infinite set of modes. However, it was shown (Figure 11) that the slowest relaxation mode with rate $\Gamma_1(q)$ and intensity $I_1(q)$ is strongly dominant in the experimentally relevant regime $q \sim q^*$ if the polydispersity degree is not too low, i.e., for $\delta_f = M_w/M_n - 1 \geqslant 0.1$. The theoretical predictions for the second mode, with rate $\Gamma_2(q)$ and intensity $I_2(q)$, are discussed in Appendix B in comparison to the data for the weak intermediate process (faster than the dominant mode and slower than the cooperative diffusion) observed in Figure 4. Once more, one should emphasize that it is not possible to distinguish and assign the two modes as the "internal" and "polydispersity" modes in this regime. It is the dominant mode (the slowest one) that incorporates the features of both: the underlying main relaxation process is the interdiffusion of compositionally heterogeneous block copolymers in the low-q regime whereas it is the internal breathing copolymer motion for $q \sim q^*$ with a transition between these two regimes.

The relaxation behavior is even more interesting for the case of weak composition polydispersity: $\delta_f < 0.1$. The genuine polydispersity mode does exist only as $\delta_f \to 0$: its intensity $I_p(q)$ is proportional to polydispersity degree δf, and hence, $I_p(q)$ is low whereas its relaxation rate $\Gamma_p(q)$ does not show any critical retardation (see dash−dot−dot−dash line in Figure 9); in fact $\Gamma_p(q)$ does not depend on the interaction parameter χ^* at all. For a small finite δf, the composition relaxation dynamics can be described in terms of two competing modes. The first ($k = 1$, slowest) mode is close to the genuine polydispersity mode for $q < q_1$; hence, its intensity $I_1(q)$ is low and nearly q-independent in the low-q regime. Above q_1, the $k = 1$ slowest mode switches behavior that closely resembles the genuine internal mode (for a monodisperse copolymer); hence, its intensity grows abruptly above q_1, and it attains a peak in the critical regime $q \approx q^*$. As the wavevector q further increases up to q_2, the first mode switches back to the behavior characteristic of the genuine polydispersity mode; i.e., $I_1(q)$ drops abruptly for $q > q_2$. The second ($k = 2$, faster) mode follows the behavior characteristic of the genuine internal mode for $q < q_1$ (its intensity $I_2(q)$ is proportional q^2 there), it follows the genuine polydispersity mode for $q_1 < q < q_2$ (hence $I_2(q)$ decreases in this regime), and it follows the internal mode again for $q > q_2$. Considering the q dependence of the mean (log-averaged) relaxation rate for weak polydispersity, $\delta_f \ll 1$, one can point out the following. The mean rate $\bar{\Gamma}(q)$, defined in eq 14a, nearly coincides with the rate of the dominant relaxation mode. Hence, $\bar{\Gamma}(q) \cong D_s q^2$ for $q < q_0 \cong \sqrt{6\delta_f} R_g^{-1}$, where $q_0 \ll q^*$ is defined by the condition $I_1(q_0) = I_2(q_0)$; see Figure 9a. It is the second (internal) mode that dominates just above q_0; hence, $\bar{\Gamma} \cong \Gamma_2 \cong \pi^2/t^* = t_d^{-1}$ for $q_0 < q \ll q^*$. Therefore, the log-averaged relaxation rate $\bar{\Gamma}(q)$ is predicted to increase sharply by a large factor $\pi^2(12\delta_f)^{-1}$ in the region $q \sim q_0$. Note that the relevant characteristic length scale $\lambda_0 = 1/q_0$ is much larger than the coil size R_g if $\delta_f \ll 1$. For $q > q_0$, the mean relaxation rate $\bar{\Gamma}(q)$ nearly coincides with $\Gamma_{i,\mathrm{mono}}(q)$, which was shown in Figure 9b.

VI. Concluding Remarks

Photon correlation spectroscopy has been used to investigate the relaxation of composition fluctuations in disordered semidilute solutions of ultrahigh molecular weight symmetric diblock copolymers in a nonselective good solvent for wavevectors q in the vicinity and on both sides of the wavevector at the maximum of the static structure factor, $q^* \sim O(1/R_g)$. The use of ultrahigh molecular weight diblocks in solution permits the investigation of the dynamic structure factor $S(q,t)$ by dynamic light scattering for $0.2 \leq q/q^* \leq 2.1$ over a wide time range ($10^{-7}-10^3$ s) as a function of copolymer concentration when approaching the ODT. It is proven that the most probable composition fluctuations with finite length scales $2\pi/q^*$ are long-lived, exhibiting a significant retardation when the ODT is approached. Actually, these short-range composition fluctuations relax slower than the ones of long range. A general

theory has also been presented for the dynamic structure factor of entangled polydisperse diblock copolymers in melt and in solution in the framework of the random phase approximation assuming reptational dynamics. It has been demonstrated that composition polydispersity is responsible for an apparent coupling of the modes of relaxation of composition fluctuations, especially near q^*. For low wavevectors, the two slower modes correspond indeed to the well-investigated "internal" and "polydispersity" modes, whereas at higher wavevectors intramolecular breathing motions (internal diffusion) and ordinary interdiffusion are coupled: both types of molecular motions may significantly contribute to the slowest relaxation mode. The theoretical results compare very favorably with the experimental data.

Acknowledgment. S.H.A. and A.N.S. acknowledge that part of this research was sponsored by NATO's Scientific Affairs Division in the frameworks of the Science for Stability and Science for Peace Programmes and by the Greek General Secretariat of Research and Technology. V.A.P. and A.N.S. acknowledge partial support by the EPSRC (Grant GR/L70851). G.F. acknowledges the financial contribution of the European Union (Grant FMRX-CT97-0112).

Appendix A

In the classical reptation model, entanglements of a given chain with the surrounding chains are assumed to create an effective tube confining the chain. Thus, the confined chain is considered as a super chain of N/N_e topological blobs with N_e monomers per blob. (In solution $N_e = N_e(\phi)$ is the mean number of links between entanglements at concentration ϕ.) The tube diameter, d_e, is equal to the size of a topological blob, $d_e = bN_e^{1/2}$ (b is the statistical segment), and the tube length is $L_t = d_e(N/N_e)$. The principal chain motion on scales larger than d_e is a reptation along the tube axis that is, in fact, one-dimensional curvilinear diffusion with diffusion constant $D_t = kT/(N\zeta_0)$, where ζ_0 is the friction constant per monomer. Neglecting the tube length fluctuations, it is assumed that the curvilinear distance between any two links, n and n', is constant, $s(n) - s(n') = L_t(n - n')/N$. During a short time δt, the nth link diffuses along the tube over a distance δs, to the point where the $(n + \delta n)$th link was originally located, with $\delta n = (N/L_t)\delta s$, $\langle(\delta s)^2\rangle = 2D_t\delta t$, and $\langle(\delta n)^2\rangle = 2D^*\delta t$, where $D^* = D_t(N/L_t)^2$. Therefore, the distribution function, $f_n(\mathbf{r},t)$, for the position $\mathbf{r}$ of the nth link obeys the diffusion equation

$$\frac{\partial f_n(\mathbf{r},t)}{\partial t} = D^* \frac{\partial^2 f_n(\mathbf{r},t)}{\partial n^2} \tag{A1}$$

Note that eq A1 is valid for a system with no excluded-volume interactions, i.e., when there is no molecular (or external) field which could affect the reptation process. The reptation model implies that the very end parts of the chains relax extremely fast, and hence, $f_n(\mathbf{r},t)$ at the ends must obey the Edwards boundary conditions,[26] $\partial f_n(q,t)/\partial n = \pm(b^2q^2/6)f_n(q,t)$ with "+" for $n = 0$ and "−" for $n = N$. Here, $f_n(q,t) = \int f_n(\mathbf{r},t)\exp(-i\mathbf{q}\cdot\mathbf{r})\,d\mathbf{r}$.

Using eqs 7−10, one can write for the symmetric polydisperse diblock

$$S^{(0)}(q,p) = \frac{\phi}{2}\int_{-1}^{1}\{S_{11}^{(0,f)}(q,p) - S_{12}^{(0,f)}(q,p)\}F(f)\,df \tag{A2}$$

$$S_{ij}^{(0,f)}(q,t) = \frac{1}{N}\int f_{nm}(q,t)\,h_i(n,f)\,h_j(m,f)\,dn\,dm \tag{A3}$$

where $f_{nm}(q,t)$ is a Fourier transformation of $f_{nm}(\mathbf{r},t)$, the probability density that the nth monomer of a given chain is at point $\mathbf{r}$ at moment t under the condition that the mth monomer was at the origin $\mathbf{r} = 0$ at $t = 0$; $h_i(n,f) = 1$ if the n-th segment is type 1 and $h_i(n,f) = 0$ otherwise: $h_1(n,f) = H(1 + f - 2n/N)$ and $h_2(n,f) = 1 - h_1(n,f)$.

Using eqs 7, A3 one gets

$$\kappa_{ij}^{(0,f)}(q,p) = \frac{1}{N}\int[f_{nm}(q,t)|_{t=0} - pf_{nm}(q,p)]h_i(n,f)\,h_j(m,f)\,dn\,dm \tag{A4}$$

where $f_{nm}(q,p) = \int_0^\infty f_{nm}(q,t)\exp(-pt)\,dt$. The function $f_{nm}(\mathbf{r},t)$ must obviously obey eq A1, with m being a parameter, with the initial condition $f_{nm}(q,t=0) = \exp[-|n - m|q^2b^2/6]$. Equation A1 can be solved using the Laplace transformation, resulting in

$$f_{nm}(q,p) = t^*\tilde{f}_{ss'}(u,\sigma) \tag{A5a}$$

with

$$\tilde{f}_{ss'}(u,\sigma) = \frac{2}{\sigma}\left[\frac{\sigma e^{-u|s-s'|} - ue^{-\sigma|s-s'|}}{2(\sigma^2 - u^2)} + u\left(\frac{\cosh(s\sigma)\cosh(s'\sigma)}{\sigma^2 - u^2 - e^\sigma(u+\sigma)^2} - \frac{\sinh(s\sigma)\sinh(s'\sigma)}{\sigma^2 - u^2 + e^\sigma(u+\sigma)^2}\right)\right] \tag{A5b}$$

$u \equiv Q^2 \equiv (qR_g)^2 = q^2Nb^2/6$ (see ref 36), $\sigma^2 = pt^*$, $t^* \equiv N^2/D^*$ is proportional to the disentanglement time $t_d = t^*/\pi^2$ (see ref 36), $s = n/N - 1/2$, and $s' = m/N - 1/2$.

Introducing a shortcut, $\kappa_0(s,s') = \exp(-u|s - s'|) - \sigma^2\tilde{f}_{ss'}(u,\sigma)$, for the expression in square brackets in eq A4, one gets

$$\kappa_0(s,s') = u\left[\frac{\sigma e^{-\sigma|s-s'|} - ue^{-u|s-s'|}}{\sigma^2 - u^2} - 2\sigma\left(\frac{\cosh(s\sigma)\cosh(s'\sigma)}{\sigma^2 - u^2 - e^\sigma(\sigma+u)^2} - \frac{\sinh(s\sigma)\sinh(s'\sigma)}{\sigma^2 - u^2 + e^\sigma(\sigma+u)^2}\right)\right] \tag{A6}$$

Using eqs A4−A6, the matrix of the ideal susceptibilities of a diblock copolymer of type f, $\kappa_{ij}^{(0,f)}(q,p)$, are calculated as

$$\kappa_{11}^{(0,f)}(q,p) = N\int_{-1/2}^{f/2}\int_{-1/2}^{f/2}\kappa_0(s,s')\,ds\,ds' = \frac{2N\left\{\left[1 - \exp\left(-\frac{(1+f)\sigma}{2}\right)\right]u - \left[1 - \exp\left(-\frac{(1+f)u}{2}\right)\right]\sigma\right\}}{\sigma(u^2 - \sigma^2)} + \frac{2Nu\left\{\frac{[\cosh(\sigma/2) - \cosh(f\sigma/2)]^2}{\sigma - u + e^\sigma(u+\sigma)} + \frac{[\sinh(\sigma/2) + \sinh(f\sigma/2)]^2}{u - \sigma + e^\sigma(u+\sigma)}\right\}}{\sigma(u+\sigma)} \tag{A7a}$$

$$\kappa_{22}^{(0,f)}(q,p) = \kappa_{11}^{(0,-f)}(q,p) \tag{A7b}$$

$$\kappa_{12}^{(0,f)}(q,p) = N\int_{f/2}^{1/2}\int_{-1/2}^{f/2}\kappa_0(s,s')\,\mathrm{d}s\,\mathrm{d}s' = \frac{Nu\left\{\frac{\sigma}{u}\Psi(u) - \Psi(\sigma) + \frac{2[\cosh(\sigma/2) - \cosh(f\sigma/2)]^2}{1 - e^{\sigma}(u+\sigma)/(u-\sigma)} + \frac{\cosh(\sigma) - \cosh(f\sigma)}{1 + e^{\sigma}(u+\sigma)/(u-\sigma)}\right\}}{\sigma(u^2 - \sigma^2)} \quad \text{(A7c)}$$

where $\Psi(x) = 1 + e^{-x} - e^{(f-1)x/2} - e^{-(f+1)x/2}$.

The susceptibility of an "ideal" bidisperse system (defined in section IV.1) is calculated using eq 10 with the distribution $F(f)$ of eq 5 and utilizing eqs A7:

$$\kappa_{bi}^{(0)}(q,p) = \frac{\phi}{4}[\kappa_{11}^{(0,f')}(q,p) + \kappa_{11}^{(0,-f')}(q,p) - 2\kappa_{12}^{(0,f')}(q,p)] = \frac{\phi Nu}{2\sigma(u^2-\sigma^2)}\left\{\sigma[\Psi_1(\sigma) - \Psi_1(u)] + 4\left[\frac{[\cosh(\sigma/2) - \cosh(f'\sigma/2)]^2}{e^{\sigma}(u+\sigma)/(u-\sigma) - 1} + \frac{[\sinh(f'\sigma/2)]^2}{e^{\sigma}(u+\sigma)/(u-\sigma) + 1}\right]\right\} \quad \text{(A8)}$$

where $\Psi_1(x) = x^{-1}[3 + e^{-x} - 2e^{-(1+f')x/2}(1 + e^{f'x})]$.

Equation A8 is used for the calculation of the susceptibility of a polydisperse system, $\kappa_{poly}^{(0)}(q,p)$, in eq 15.

Appendix B

In section IV, a general theory is presented for the relaxation of composition fluctuations in a polydisperse copolymer system. An infinite series of relaxation modes are predicted, with the slowest one ($k = 1$) strongly dominating in the experimentally relevant regime $q \sim q^*$ for polydispersity degrees $\delta_f = M_w/M_n - 1 \geq 0.1$. The next faster mode (with $k = 2$) exhibits much weaker intensity but may be experimentally resolved; even faster modes ($k = 3, 4, \ldots$) exhibit too low intensities. The dependence of the intensity and relaxation rate of the two slower modes on the wavevector, q, the degree of composition polydispersity, δf, and the relative distance from the disorder-to-order transition, ϵ, was demonstrated in Figures 10 and 11. It was shown there that the thermodynamic interactions as well as the polydispersity affect mostly the slowest ($k = 1$) dominant mode. The more than 1 order of magnitude lower intensity of the $k = 2$ mode (even much lower near the transition and/or at low wavevectors) makes it very difficult for the second mode to be resolved for real systems.

Nevertheless, for both copolymers at concentrations where the systems are entangled (i.e., for concentrations such that $N > 2N_e(\phi)$, with $N_e(\phi)$ the number of links between entanglements at concentration ϕ), a very weak process was observed with relaxation time faster than that of the main mode. This can be seen in Figure 4, where, besides the fast cooperative diffusion and the slow dominant mode (discussed above), there is another intermediate process. The significantly lower intensity of the intermediate mode compared to the main one is evident, especially for wavevectors $q \sim q^*$ or in the low-q regime. The relaxation times of the two processes are always different by more than 1 decade (depending on the wavevector). To quantitatively discuss the characteristics of the intermediate mode, one has to emphasize from the beginning the significant errors associated with its intensity and dynamics due to the very high intensity of the dominant mode. However, as can also be seen in Figure 13, the intensity of the process is increasing with q in the low-q regime (with the intensity apparently going to zero as $q \to 0$), whereas its rate is apparently q-independent. (It is certainly not influenced by q^*.) Moreover, the mode becomes slightly stronger and slower with increasing the concentration, whereas none of its characteristics appear to be influenced by the proximity to the ODT. Figure 13 shows the intensities and the rates of the slower (the dominant) and the intermediate of the experimentally resolved processes for the 2.52 wt % SI-3M50 toluene solution (the even faster cooperative diffusion is not shown), where the features discussed for their wavevector dependencies are seen.

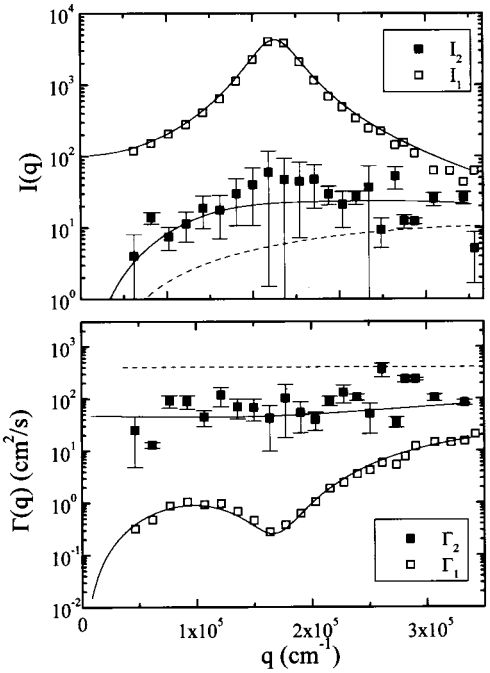

Figure 13. Wavevector dependence of (a) the intensities $I(q)$ and (b) the relaxation rates $\Gamma(q)$ of the two slower relaxation processes observed for a 2.52 wt % SI-3M50 toluene solution at 20 °C. The solid lines are the theoretical predictions based on eqs 13, 8, and 16 for the $k = 1$ and $k = 2$ modes. The dashed lines are the theoretical calculations based on eqs B1−B3 for the $l = 1$ Rouse mode.

These features of the faster process resemble the theoretical predictions for the $k = 2$ mode (discussed in relation to Figures 10 and 11), so an attempt is made to compare it to the experimental results. In Figure 13, the theoretical predictions are shown for the $k = 1$ and $k = 2$ modes. It is stressed that the theoretical curves were calculated using exactly the same parameters obtained from the analysis of the main dominant mode, discussed in section V and shown in Figure 12. It is evident that the model quantitatively captures the characteristics of the faster process as well.

Alternatively, one may identify this intermediate process with the Rouse mode discussed earlier[12] due to curvilinear chain fluctuations within their reptation tubes. In the entangled regime, the motion of a polymer chain is always a combination of reptation and Rouse-like motions. For entangled monodisperse diblock copolymers and for $q \leq q^*$, the contribution to the dynamic structure factor due to Rouse-like motions within the tube was calculated as[12]

$$S_R(q,t) = \frac{N_e(\phi)\phi}{6\pi^2}\sum_l J_l(u)\exp[-tl^2/\tau_R] \qquad \text{(B1)}$$

τ_R is the Rouse time of a linear chain with $N/N_e(\phi)$ topological blobs, for which $t_d/\tau_R = 3N/N_e(\phi)$, i.e., $\tau_R = (t^*/3\pi^2)[N_e(\phi)/N]$ (since $\tau_d = t^*/\pi^2$), l is a positive integer, and

$$J_l(u) = (u/l^2)[1 - 2uM_l(u^2 + \pi^2 l^2)^{-2}] \qquad \text{(B2)}$$

with $u = q^2R_g^2$,[12,36] and M_l given by

$$M_l = (u/2 + 2)(u^2 + \pi^2 l^2) - 3u^2 + u^2 e^{-u} + 4\pi u l e^{-u/2}(-1)^{(l+1)/2}; \quad l = \text{odd}$$

$$= (u/2)(u^2 + \pi^2 l^2) - 3u^2 - u^2 e^{-u} + 4u^2 e^{-u/2}(-1)^{l/2}; \quad l = \text{even} \qquad \text{(B3)}$$

The comparison of the predictions for the first Rouse mode ($l = 1$) with the experimental data for the intermediate process is also shown in Figure 13. It is again noted that the parameters obtained from the analysis of the dominant mode are used for these calculations. The characteristics of the process are similar to those of the data; however, the predictions underestimate the intensity and overestimate the rate by a factor of about 4. Inclusion of faster modes ($l = 2$, 3, ...) by calculating the total intensity of all Rouse modes and a log-averaged rate (similarly to eq 14a) improves the comparison of the intensities but worsens that for the rates.

Therefore, it appears that the intermediate process observed is the $k = 2$ mode of a compositionally polydisperse diblock copolymer, which for the range of parameters in the present system (δf, $q \sim q^*$ $\epsilon(\phi)$) exhibits intensity significantly lower than that of the $k = 1$ mode. It is once more noted that, although in the $qR_g \to 0$ regime the two modes observed earlier[8−10,16,17] can be definitely assigned to the "internal" and the "polydispersity" modes contributing to the dynamic structure factor (in agreement with the limiting behavior of the theoretically predicted modes for a polydisperse diblock), it is the very high intensity of the slower mode for the present δf and for the present range of $q \sim q^*$ and $\epsilon(\phi)$ that hinders the definite identification of the second mode.

References and Notes

(1) Sillescu, H. *Makromol. Chem., Rapid Commun.* **1984**, *5*, 519; *Makromol. Chem., Rapid Commun.* **1987**, *8*, 393. Composto, R. J.; Mayer, J. W.; Kramer, E. J.; White, D. M. *Phys. Rev. Lett.* **1986**, *57*, 1312. Jones, R. A. L.; Klein, A.; Donald, A. M. *Nature* **1986**, *321*, 161. Fytas, G. *Macromolecules* **1987**, *20*, 1430. Green, P. F.; Doyle, B. L. *Macromolecules* **1987**, *20*, 2471. Kanetakis, J.; Fytas, G. *Macromolecules* **1989**, *22*, 3452. Meier, G.; Fytas, G.; Momper, B.; Fleischer, G. *Macromolecules* **1993**, *26*, 5310 and references therein.

(2) Leibler, L. *Macromolecules* **1980**, *13*, 1602. Fredrickson, G. H.; Helfand, E. *J. Chem. Phys.* **1987**, *87*, 697. Barrat, G. L.; Fredrickson, G. H. *J. Chem. Phys.* **1991**, *95*, 1282.

(3) Bates, F. S.; Fredrickson, G. H. *Annu. Rev. Phys. Chem.* **1990**, *41*, 525. Bates, F. S. *Science* **1991**, *251*, 898.

(4) Erukhimovich, I. Ya.; Semenov, A. N. *Zh. Eksp. Teor. Fiz.* **1986**, *63*, 259 [*Sov. Phys. JETP* **1986**, *28*, 149].

(5) Akcasu, A. Z.; Benmouna, M.; Benoit, H. *Polymer* **1986**, *27*, 1935. Benmouna, M.; Benoit, H.; Borsali, R.; Duval, M. *Macromolecules* **1987**, *20*, 2620. Akcasu, A. Z.; Tombakoglu, M. *Macromolecules* **1990**, *23*, 607. Borsali, R.; Vilgis, T. A. *J. Chem. Phys.* **1990**, *93*, 3610. Borsali, R.; Fischer, E. W.; Benmouna, M. *Phys. Rev. A* **1991**, *43*, 5732.

(6) Borsali, R.; Benoit, H.; Legrand, J.-F.; Duval, M.; Picot, C.; Benmouna, M.; Farago, B. *Macromolecules* **1989**, *22*, 4119. Duval, M.; Picot, C.; Benoit, H.; Borsali, R.; Benmouna, M.; Lartigue, C. *Macromolecules* **1991**, *24*, 3185.

(7) Duval, M.; Haida, H.; Lingelser, J. P.; Gallot, Y. *Macromolecules* **1991**, *24*, 6867.

(8) Anastasiadis, S. H.; Fytas, G.; Vogt, S.; Fischer, E. W. *Phys. Rev. Lett.* **1993**, *70*, 2415. Vogt, S.; Anastasiadis, S. H.; Fytas, G.; Fischer, E. W. *Macromolecules* **1994**, *27*, 4335.

(9) Jian, T.; Anastasiadis, S. H.; Semenov, A. N.; Fytas, G.; Adachi, K.; Kotaka, T. *Macromolecules* **1994**, *27*, 4762.

(10) Liu, Z.; Pan, C.; Lodge, T. P.; Stepanek, P. *Macromolecules* **1995**, *28*, 3221. Pan, C.; Mauer, W.; Liu, Z.; Lodge, T P.; Stepanek, P.; von Meerwall, E. D.; Watanabe, H. *Macromolecules* **1995**, *28*, 1643.

(11) Boudenne, N.; Anastasiadis, S. H.; Fytas, G.; Xenidou, M.; Hadjichristidis, N.; Semenov, A. N.; Fleischer, G. *Phys. Rev. Lett.* **1996**, *77*, 506.

(12) Semenov, A. N.; Anastasiadis, S. H.; Boudenne, N.; Fytas, G.; Xenidou, M.; Hadjichristidis, N. *Macromolecules* **1997**, *30*, 6280.

(13) Sigel, R.; Pispas, S.; Hadjichristidis, N.; Vlassopoulos, D.; Fytas, G. *Macromolecules* **1999**, *32*, 8447.

(14) The total concentration fluctuations in semidilute solutions relax via a fast diffusive process, i.e., via the cooperative diffusion of the transient network of the overlapping polymer chains,[5,7,9−12] similarly to semidilute homopolymer solutions.

(15) Montes, H.; Monkenbusch, M.; Willner, L.; Rathgeber, S.; Fetters, L.; Richter, D. *J. Chem. Phys.* **1999**, *110*, 10188.

(16) Fytas, G.; Anastasiadis, S. H.; Semenov, A. N. *Makromol. Chem., Macromol. Symp.* **1994**, *79*, 117. Semenov, A. N.; Fytas, G.; Anastasiadis, S. H. *Polym. Prepr.* **1994**, *35* (1), 618.

(17) Jian, T.; Anastasiadis, S. H.; Fytas, G.; Fleischer, G.; Vilesov, A. D. *Macromolecules* **1995**, *28*, 2439. Jian, T.; Fytas, G.; Anastasiadis, S. H.; Vilesov, A. D. *Polym. Mater. Sci. Eng.* **1994**, *71*, 767.

(18) Fytas, G.; Anastasiadis, S. H. In *Disorder Effects on Relaxation Processes*; Richert, R., Blumen, A., Eds.; Spinger-Verlag: Berlin, 1994. Fredrickson, G. H.; Bates, F. S. *Annu. Rev. Phys. Chem.* **1996**, *26*, 503. Stepanek, P.; Lodge, T. P. In *Light Scattering*; Brown, W., Ed.; Oxford University Press: Oxford, 1996. Stepanek, P.; Lodge, T. P. In *Light Scattering and Photon Correlation Spectroscopy*; Pike, E. R., Abbiss, J. B., Eds.; Kluwer Academic Publishers: Dordrecht, The Netherlands, 1997. Chrissopoulou, K.; Rittig, F.; Fytas, G. In *Molecular Interactions and Time-Space Organization in Macromolecular Systems*; Morishima, Y., Norisuye, T., Tashiro, K., Eds.; Springer-Verlag: Berlin, 1999. Anastasiadis, S. H. *Curr. Opin. Colloid Interface Sci.* **2000**, *5*, 324.

(19) Fredrickson, G. H.; Larsen, R. G. *J. Chem. Phys.* **1987**, *86*, 1553. Fredrickson, G. H. *J. Chem. Phys.* **1986**, *85*, 5306.

(20) Benmouna, M.; Benoit, H. *J. Polym. Sci., Polym. Phys. Ed.* **1983**, *21*, 1227. Hong, K. M.; Noolandi, J. *Macromolecules* **1983**, *16*, 1083. Onuki, A.; Hashimoto, T. *Macromolecules* **1989**, *22*, 879. Olvera de la Cruz, M. *J. Chem. Phys.* **1989**, *90*, 1995.

(21) Fredrickson, G. H.; Leibler, L. *Macromolecules* **1989**, *22*, 1238.

(22) Huang, C.-I.; Lodge, T. P. *Macromolecules* **1998**, *31*, 3556.

(23) Hashimoto, T.; Kowasaka, K.; Shibayama, M.; Kawai, H. *Macromolecules* **1986**, *19*, 754. Hashimoto, T.; Mori, K. *Macromolecules* **1990**, *23*, 5347.

(24) Lodge, T. P.; Pan, C.; Jin, X.; Liu, Z.; Zhao, J.; Maurer, W. W.; Bates, F. S. *J. Polym. Sci., Part B: Polym. Phys.* **1995**, *33*, 2289. Huang, C.-I.; Chapman, B. R.; Lodge, T. P. *Macromolecules* **1998**, *31*, 9384.

(25) de Gennes, P. G. *Scaling Concepts in Polymer Physics;* Cornell University Press: Ithaca, NY, 1979.

(26) de Gennes, P. G. *J. Phys. (Paris)* **1981**, *42*, 735.

(27) Doi, M.; Edwards, S. F. *The Theory of Polymer Dynamics*; Oxford Science Publishers: Oxford, 1986.

(28) Anastasiadis, S. H.; Rittig, F.; Chrissopoulou, K.; Fleischer, G.; Fytas, G.; Semenov, A. N.; Kärger, J.; Xenidou, M.; Pispas, S.; Hadjichristidis, N. *Europhys. Lett.* **2000**, *51*, 68.

(29) Burger, C.; Ruland, W.; Semenov, A. N. *Macromolecules* **1990**, *23*, 3339.

(30) Landau, L. D.; Lifshitz, E. M. *Statistical Physics, Part I;* Pergamon: Oxford, 1980.

(31) Brochard, F.; de Gennes, P. G. *Physica A* **1983**, *118*, 289.

(32) Leibler, L.; Benoit, H. *Polymer* **1981**, *22*, 195. Hong, K. M.; Noolandi, J. *Polym. Commun.* **1984**, *25*, 265.

(33) For $q/q^* \geq 4$ (not shown), the mean relaxation rate $\bar{\Gamma}$ saturates at $\bar{\Gamma} \cong 4\pi^2/t^*$, following the faster internal mode. (As a matter of fact, the slow mode rate $\Gamma_1 \to \pi^2/t^*$ for $q \gg q^*$

in the low δf regime.) Hence, the effective diffusion constant $\bar{\Gamma}/q^2$ decreases again (as q^{-2}) for $q \gg q^*$ or, more precisely, for $4 \leq q/q^* \ll N/N_e$. Note that the last condition ($q/q^* < N/N_e$) is equivalent to $qd_e < 1$, which means that the relevant wavelength $1/q$ is longer than the tube diameter d_e; i.e., the reptation dynamics is applicable. For $q/q^* > N/N_e$, the main mode of composition relaxation follows the internal Rouse dynamics, so that $\bar{\Gamma} \sim (t^*)^{-1}(N/N_e)^3[(q/q^*)(N_e/N)]^4$ (see ref 34). Note a sharp increase of $\bar{\Gamma}$ by a factor $\sim(N/N_e)^3$ in the region $qd_e \sim 1$.

(34) Semenov, A. N. In *Theoretical Challenges in the Dynamics of Complex Fluids;* McLeish, T., Ed.; NATO ASI Series, Series E: Applied Sciences; Kluwer Academic Publishers: Dordrecht, The Netherlands, 1997; Vol. 339, pp 63−76.
(35) Lodge, T. P.; Dalvi, M. C. *Phys. Rev. Lett.* **1995**, *75*, 657. Dalvi, M. C.; Lodge, T. P. *Macromolecules* **1994**, *27*, 3487.
(36) Note that in ref 12 the variables u and t^* were defined as $u = q^2 R_g^2/2$ and $t^* \equiv N^2/(4D^*)$ whereas in the present paper $u \equiv q^2 R_g^2$ and $t^* \equiv N^2/D^*$.

MA001541B